The Nitrogen Isotopic Composition of Tissue and Shell-Bound Organic Matter of Planktic Foraminifera in Southern Ocean Surface Waters

Author(s):
Smart, Sandi M.; Fawcett, Sarah E.; Ren, Haojia; Schiebel, Ralf; Tompkins, Emily M.; Martínez-García, Alfredo; Stirnimann, Luca; Roychoudhury, Alakendra; Haug, Gerald H.; Sigman, Daniel M.

Publication date:
2020-02

Permanent link:
https://doi.org/10.3929/ethz-b-000456942

Originally published in:
Geochemistry, Geophysics, Geosystems 21(2), https://doi.org/10.1029/2019gc008440

Geochemistry, Geophysics, Geosystems

AGU100 ADVANCING EARTH AND SPACE SCIENCE

RESEARCH ARTICLE
10.1029/2019GC008440

Key Points:
- Foraminifer $\delta^{15}N$ tracks bulk particulate organic N (rather than nitrate) $\delta^{15}N$ in the Southern Ocean mixed layer on a seasonal basis
- Particulate N $\delta^{15}N$ records early-summer nitrate consumption, late-summer ammonium recycling, and winter decomposition
- With today's seasonality, late summer is estimated to outweigh winter in its effect on the $\delta^{15}N$ of foraminifera accumulated on the seabed

Supporting Information:
- Supporting Information S1

Correspondence to:
S. M. Smart,
sandi.smart@alumni.uct.ac.za

Citation:
Smart, S. M., Fawcett, S. E., Ren, H., Schiebel, R., Tompkins, E. M., Martínez-García, A., et al. (2020). The nitrogen isotopic composition of tissue and shell-bound organic matter of planktic foraminifera in Southern Ocean surface waters. *Geochemistry, Geophysics, Geosystems*, *21*, e2019GC008440. https://doi.org/10.1029/2019GC008440

Received 10 MAY 2019
Accepted 5 JAN 2020
Accepted article online 7 JAN 2020

The Nitrogen Isotopic Composition of Tissue and Shell-Bound Organic Matter of Planktic Foraminifera in Southern Ocean Surface Waters

Sandi M. Smart[1,2], Sarah E. Fawcett[3], Haojia Ren[4], Ralf Schiebel[2], Emily M. Tompkins[5], Alfredo Martínez-García[2], Luca Stirnimann[3], Alakendra Roychoudhury[1], Gerald H. Haug[2], and Daniel M. Sigman[6]

[1]Department of Earth Sciences, Stellenbosch University, Matieland, South Africa, [2]Climate Geochemistry Department, Max Planck Institute for Chemistry, Mainz, Germany, [3]Department of Oceanography, University of Cape Town, Rondebosch, South Africa, [4]Department of Geosciences, National Taiwan University, Taipei, Taiwan, [5]Department of Biology, Wake Forest University, Winston-Salem, NC, USA, [6]Department of Geosciences, Princeton University, Princeton, NJ, USA

Abstract We present the first nitrogen isotope ($\delta^{15}N$) measurements of planktic foraminifera, paleoceanographically important zooplankton, from the nutrient-rich waters of the modern Southern Ocean. Foraminifera were collected from net tows in the Subantarctic and Polar Frontal Zones (SAZ and PFZ, respectively) south of Africa during winter 2015 and late summer 2016. In late summer, consistent with preferential uptake of ^{14}N-nitrate and the progressive, northward depletion of nitrate by phytoplankton across the Southern Ocean, foraminifer tissue and shell-bound $\delta^{15}N$ rise equatorward along with nitrate $\delta^{15}N$. However, foraminifer $\delta^{15}N$ is ~3‰ lower than expected for heterotrophs relying on photosynthetic biomass generated directly from nitrate. This discrepancy appears to originate with the particulate organic N (PON) in late-summer surface waters, the $\delta^{15}N$ of which is lowered by ammonium recycling. In winter, when overall productivity and foraminifer production are reduced, foraminifer $\delta^{15}N$ is higher (by 4.6 ± 0.8‰ for tissue and by 4.0 ± 1.5‰ for shell-bound N compared to late summer) and exhibits no clear north-south trend. These characteristics can also be explained by the feeding-driven connection of foraminifera to PON, which is elevated in $\delta^{15}N$ by net degradation in winter. Therefore, foraminifer $\delta^{15}N$ is more closely tied to PON $\delta^{15}N$ than to nitrate $\delta^{15}N$ in the Southern Ocean mixed layer. Combining our isotope data with previously reported sediment trap fluxes from the western Pacific SAZ/PFZ suggests that, under modern conditions, the late-summer ammonium recycling signal outweighs that of wintertime decomposition on the annually integrated $\delta^{15}N$ of sinking foraminifera.

Plain Language Summary Shells of foraminifera, single-celled zooplankton, record information about their surroundings, making their fossils a useful tool for investigating past ocean conditions. Paleoceanographers have begun to use the ratio of heavy-to-light-nitrogen isotopes in fossil foraminifer shells as a measure of past biological nitrate consumption in the Southern Ocean. But the isotopic link between living foraminifera and the nitrate consumed has only been tested in the subtropics, where s urface nitrate is fully consumed by phytoplankton. In today's polar ocean, surface nitrate is only partly consumed and mostly during the productive spring/summer. Our goal was to investigate whether living foraminifera record the isotopic composition of nitrate consumed in Southern Ocean surface waters. We collected living foraminifera from the region south of Africa during winter and late summer, using a net towed by the ship. We found that the nitrogen in foraminifer shells and tissues most closely tracks the foraminifer's particulate nitrogen food. While nitrate and particulate nitrogen in surface waters are closely linked during spring/summer, the two can diverge because of nitrogen recycling in late summer and winter. Therefore, when interpreting foraminifer-bound nitrogen isotope paleo-records, we must consider the effects of these "off-peak" seasons, as their influence may have been different at certain times in the past.

1. Introduction

The Southern Ocean is the world's largest surface-ocean reservoir of unused nitrate, a major nutrient for phytoplankton, and the region has the capacity for far greater productivity and carbon sequestration than

occurs today (Knox & McElroy, 1984; Sarmiento & Toggweiler, 1984; Siegenthaler & Wenk, 1984). One way to monitor the degree of nitrate (and, indirectly, carbon) drawdown by phytoplankton is through the use of nitrogen (N) isotopes. During its consumption by phytoplankton, nitrate containing the lighter ^{14}N isotope is preferentially consumed over ^{15}N-bearing nitrate, producing particulate organic N (PON) with a low $\delta^{15}N$ while raising the $\delta^{15}N$ of the residual nitrate (where $\delta^{15}N = \{[(^{15}N/^{14}N)_{sample}/(^{15}N/^{14}N)_{N2\ in\ air}] - 1\} \times 1{,}000$; in units of per mil, ‰). As consumption proceeds, both reactant (nitrate) and product (PON) $\delta^{15}N$ rise (Pennock et al., 1996; Sigman, Altabet, McCorkle, et al., 1999; Wada & Hattori, 1978; Waser et al., 1998). These dynamics are reflected in the $\delta^{15}N$ of the organic N that is exported as sinking material from the surface ocean and accumulates in deep sea sediments, raising the prospect of reconstructing past changes in surface-ocean nitrate drawdown from the $\delta^{15}N$ of PON buried in seafloor sediments (Altabet & François, 1994; François et al., 1992). However, bulk PON is poorly preserved in Southern Ocean sediments, compromising its use for paleo-$\delta^{15}N$ reconstructions (Altabet & François, 1994; Robinson et al., 2012, and references therein).

Microfossil-bound organic matter offers a physically protected subpool of the sedimentary organic matter, with a $\delta^{15}N$ that should be less vulnerable to diagenetic alteration or sedimentary contamination (Ren et al., 2009; Robinson et al., 2004; Sigman, Altabet, François, et al., 1999). In the Antarctic Zone (AZ), south of the Polar Front (PF), the silica frustules of diatoms (single-celled algae) have been used for this purpose (Robinson et al., 2004; Sigman, Altabet, François, et al., 1999; Studer et al., 2015; Studer et al., 2018). In more northern latitudes of the Southern Ocean, which are the focus of our study, a promising microfossil candidate is the planktic foraminifer, a single-celled zooplankton with a calcium carbonate shell or "test" (Martínez-García et al., 2014). Foraminifera use N-rich proteins to construct calcite chambers, which are added periodically to the shell during its lifetime (ranging from 2 weeks to 1 year, depending on the species; Bé et al., 1979; Hemleben et al., 1989; King & Hare, 1972; Spero, 1988). Additional calcite added either actively during development (ontogenesis) and reproduction (gametogenesis), or passively during burial (i.e., postmortem encrustation; Bé & Hemleben, 1970; Hemleben et al., 1985) can further protect this shell-bound organic matter from bacterial decomposition.

Planktic foraminifera do not migrate diurnally (Meilland et al., 2019; Schiebel & Hemleben, 2017; Siccha et al., 2012), but many species may undertake large depth changes during a specific stage of life (e.g., for reproduction; Hemleben et al., 1985; Schiebel, 2002; Schiebel & Hemleben, 2017). In laboratory feeding experiments, most spinose species (e.g., *Orbulina universa*, *Trilobatus sacculifer*) have been observed to readily accept zooplankton prey like copepods and sometimes also larger phytoplankton like diatoms, while most nonspinose species (e.g., *Globorotalia truncatulinoides*, *Globorotalia inflata*, *Globorotalia hirsuta*) appear to prefer algal prey and/or detrital organic matter (Anderson et al., 1979; Spindler et al., 1984). Bacterial food sources (abundant in the ocean but not offered in feeding experiments) might be important for some species, including the spinose *Globigerina bulloides* (Bird et al., 2017) and the nonspinose *Neogloboquadrina incompta* (Bird et al., 2018). Shell geochemistry (specifically, Ba/Ca ratios) suggests a "marine snow" habitat for the nonspinose, intermediate-depth dwelling *Neogloboquadrina dutertrei* (Fehrenbacher et al., 2018), where it apparently feeds on other inhabitants (in this case, protists) of the organic aggregate (Bird et al., 2018).

In the low-to-mid-latitude oceans, many spinose, shallow-dwelling species (e.g., *O. universa*, *T. sacculifer*, *Globigerinoides ruber*) are known to host intracellular dinoflagellate symbionts (e.g., Bé et al., 1977; Spero, 1987; and references therein). In return for metabolic ammonium and phosphate from the host, these symbionts photosynthesize and transfer a portion of the resulting organic matter to the foraminifer (Uhle et al., 1999), supplementing the organic carbon that it obtains from its largely carnivorous diet (Anderson et al., 1979; Spindler et al., 1984). These dinoflagellate-bearing foraminifera appear to depend on their photosymbionts for survival (i.e., "obligatory" symbiosis; Hemleben et al., 1989), such that they are functionally mixotrophic rather than heterotrophic (Le Kieffre et al., 2018; Stoecker et al., 2009; Stoecker et al., 2017). Some of these (sub)tropical foraminifer species (e.g., *O. universa*) also occur in the Subantarctic Zone (SAZ; between the Subantarctic Front, SAF, and the Subtropical Front, STF; King & Howard, 2003; Mortyn & Charles, 2003). In the Polar Frontal Zone (PFZ; between the PF and the SAF), elevated foraminiferal abundances (of *G. bulloides*, in particular) have been observed at the depth of the subsurface chlorophyll maximum (Mortyn & Charles, 2003). Unlike the (sub)tropical spinose species discussed

above, *G. bulloides* and *Turborotalita quinqueloba* (temperate/subpolar and polar/subpolar species, respectively, and both spinose) have not been reported to host dinoflagellate endosymbionts (Gastrich, 1987; Hemleben et al., 1989; Schiebel & Hemleben, 2017) or to contain functional (i.e., nonfood derived) chlorophyll (Takagi et al., 2019). While associations of *G. bulloides* with cyanobacterial endosymbionts (Bird et al., 2017) and free-swimming dinoflagellates (Spero & Angel, 1991) have been documented, it is not yet clear how pervasive these relationships are. Several intermediate-depth dwellers (including *G. inflata*, *Globigerinita glutinata*, *G. hirsuta*, and *N. dutertrei*) are suspected to host chrysophyte or pelagophyte symbionts, while the deepest-dwelling planktic foraminifer (*G. truncatulinoides*) and native polar/subpolar species (*Neogloboquadrina pachyderma* and *N. incompta*) appear to be symbiont-barren (Bird et al., 2018; Faber et al., 1988; Gastrich, 1987; Takagi et al., 2019). In terms of $\delta^{15}N$, a clear distinction has been observed between species that host dinoflagellate endosymbionts and those that do not; the former group has a significantly lower $\delta^{15}N$, explained as deriving from the recycling of low-$\delta^{15}N$, metabolic ammonium from the host (Ren et al., 2012; Smart et al., 2018).

In the tropical and subtropical oceans, spatial variations in the shell-bound $\delta^{15}N$ of recently deposited foraminifera appear to track the $\delta^{15}N$ of the thermocline nitrate supplied annually to overlying surface waters (Ren et al., 2009; Ren et al., 2012; Schiebel et al., 2018). This is consistent with the complete or near-complete consumption of nitrate in the modern euphotic zone of these regions on an annual basis (Altabet, 1988; François et al., 1992). On shorter (i.e., seasonal) time scales, however, the $\delta^{15}N$ of bulk foraminifer tissue (i.e., the noncalcified biomass of living foraminifera caught in surface net tows) and sinking shells (intercepted by sediment traps) also reflects changes in upper ocean N recycling (Smart et al. (2018)). In the Southern Ocean, nitrate supplied to the mixed layer is not fully consumed by phytoplankton, so we expect the degree of nitrate consumption to represent a major influence on the $\delta^{15}N$ of the biomass produced in surface waters and thus to also affect foraminifer $\delta^{15}N$. In addition to the degree of nitrate consumption by phytoplankton, the $\delta^{15}N$ of nitrate in the mixed layer depends on the $\delta^{15}N$ of the nitrate supply and the isotope effect of nitrate assimilation (Altabet & François, 1994; Sigman, Altabet, McCorkle, et al., 1999). Based on these expectations, a foraminifer-bound $\delta^{15}N$ record from the SAZ has been generated to reconstruct nitrate consumption through the last glacial cycle (Martínez-García et al., 2014), but the link between foraminifer $\delta^{15}N$ and nitrate $\delta^{15}N$ has not yet been demonstrated in the modern Southern Ocean.

Here, through $\delta^{15}N$ measurements of foraminifera (tissue and shells), nitrate, and various particulate N forms, we seek to determine whether upper ocean-dwelling foraminifera in the modern PFZ and SAZ track the $\delta^{15}N$ of the nitrate and thus the degree of nitrate consumption. We find that foraminifer $\delta^{15}N$ is tied to the $\delta^{15}N$ of PON in the mixed layer, a predictable result given that foraminifera are known to feed on this material. The $\delta^{15}N$ of PON is largely controlled by nitrate consumption in the early and midsummer (Lourey et al., 2003), but we confirm previous findings that ammonium cycling and decomposition cause significant overprints on PON $\delta^{15}N$ in late summer and winter, respectively (Altabet & François, 2001; Lourey et al., 2003). These overprints are also recorded in foraminifer $\delta^{15}N$, causing them to deviate from recording nitrate consumption alone during the low-flux late-summer and winter periods. We provide an initial exploration of the significance of these findings for the foraminifer-bound $\delta^{15}N$ proxy in the Southern Ocean.

2. Methods

2.1. Sample Collection at Sea

Planktic foraminifera were collected from the Southern Ocean using a double 1-m^2-opening, 200-μm-mesh plankton net in July-August (winter) 2015 (Atlantic sector, between South Africa and the Antarctic sea-ice edge at 56.4°S, 0.3°E; Figure 1a) and in April-May (late summer) 2016 (Indian sector, between South Africa and Marion Island at 46.9°S, 37.7°E; Figure 1b) aboard the R/V *S.A. Agulhas II* (VOY016 and VOY019, respectively). The positions of the major Southern Ocean fronts were determined from expendable bathythermograph temperature and salinity profiles (using the criteria of Belkin & Gordon, 1996, and Holliday & Read, 1998) in winter 2015. On the late-summer 2016 voyage, the fronts were identified from gradients in continuous surface temperature and salinity (underway thermosalinograph) measurements and altimetry (Aviso Absolute Dynamic Topography; https://www.aviso.altimetry.fr). Before net deployment, hydrographic profile data and seawater nitrate samples were collected from a Niskin bottle rosette mounted with Sea-Bird conductivity-temperature-depth (CTD) and florescence sensors. Mixed-layer depth was

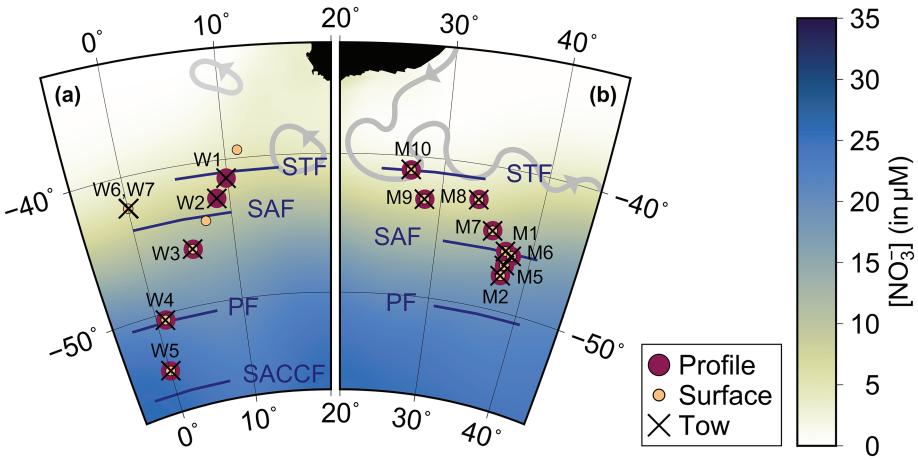

Figure 1. Cruise tracks of the R/V *S.A. Agulhas II* during (a) winter 2015 along the Good Hope Line (0°E) and (b) late summer 2016 to Marion Island (46.9°S, 37.7°E). Each net tow is marked by a black "x" and named by cruise ("W" for winter, "M" for Marion) and tow number. Stations sampled for seawater nitrate and particulate organic N are indicated by filled circles (underway surface stations in orange and depth profile stations in maroon). Each cruise track is overlaid on its monthly climatology (July and April, respectively) of surface nitrate concentration (in µM; color shading) from World Ocean Atlas 2013 (Garcia et al., 2014; online at https://www.nodc.noaa.gov/OC5/woa13/). The relevant oceanic fronts at the time of sampling are indicated (STF: Subtropical Front, SAF: Subantarctic Front, PF: Polar Front, and SACCF: Southern Antarctic Circumpolar Current Front). Thick gray lines show the approximate circulation of the Agulhas Current (western boundary of the south Indian Ocean), Agulhas Retroflection (eastward return flow) and rings (warm-core eddies shed into the southeast Atlantic) based on altimetry at the time of each cruise. This figure was created using GMT (Wessel et al., 2013).

defined as the minimum depth at which potential density (σ_θ, calculated from temperature and salinity profiles) increased by ≥0.03 kg/m^3 from a reference depth of 11 m, the shallowest depth common to all CTD stations (de Boyer Montégut et al., 2004).

Net tows were performed at 14 different sites: six in winter, eight in late summer. Each tow lasted approximately 90 min, with the net towed at 1–1.5 kn at a depth between 25 and 90 m (see Table S1 in the supporting information for details), targeting the chlorophyll maximum (or the middle of the mixed layer if the fluorescence profile was relatively homogenous). Once retrieved, approximately 90% of the foraminifer-containing tow material was preserved in a 5–10% formalin-seawater solution (pH-buffered with sodium borate) and kept at 4 °C until processing (following Ren et al., 2012). The remaining 10% was sieved (through 5,000-; 2,000-; 1,000-; 500-; 250-; and 150-µm-mesh sieves), filtered (onto precombusted 0.7-µm-pore-size GF/Fs) and frozen at −20 °C for elemental and isotopic analysis of size-fractionated PON. For the duration of each tow, seawater from the ship's underway intake (at ~7-m depth) was filtered through a new precombusted 0.3-µm-pore-size GF/F in order to collect bulk PON and filtered nitrate from surface waters. GF/Fs were frozen at −80 °C and all nitrate samples (from profile and underway collections) were frozen at −20 °C until analysis. Additional bulk PON samples from the region (35–57°S and 0–42°E) come from underway surface and CTD profile collections in July-August (winter) 2012 (VOY03; R/V *S.A. Agulhas II*), February-March (late summer) 2013 (SOSCEx I; R/V *S.A. Agulhas I*), December-March (midsummer) 2016/2017 (ACE; R/V *Akademik Treshnikov*), and June-July (winter) 2017 (VOY025; R/V *S.A. Agulhas II*).

2.2. Foraminifer Sample Preparation, Cleaning and Oxidation

Foraminifera were separated from bulk formalin-preserved tow material by sieving (using a 500- or 1,000-µm-mesh sieve and rinsing with deionized water), density separation (addition of a 200 g/L sodium chloride solution), decanting into petri dishes, and allowing the diluted formalin solution to evaporate in a fume hood (adapted from Smart et al., 2018). For some tows, an additional separation step was needed; dried material was resuspended (in tap water, adjusted to pH ~8 using 2–3 drops of 1 N sodium hydroxide) and gently disaggregated in a recrystallizing dish, swirled and allowed to settle. Foraminifera and other dense particles, which accumulate at the center of the dish, could be pipetted off under a microscope and transferred to a clean petri dish to dry at room temperature. This swirl-and-pipette step was repeated until

no more foraminifera were visible at the center of the dish. Nine different species were identified and picked from the dried material in the petri dishes under a microscope using a wet picking brush. Depending on their abundance, size, and estimated N content (based on preceding measurements; supporting information Text S3 and Tables S2 and S3), specimens were earmarked for tissue (typically 1–50 individuals) and/or shell-bound (typically 50–150 individuals) N isotope analysis, and if possible, sorted into size fractions using a microscope reticle.

Subsequent laboratory work was undertaken during three different sessions: in 2016, 2017 (at Princeton University, USA), and 2018 (at the Max Planck Institute for Chemistry [MPIC], Germany). During each session, different protocols were tested for the processing (i.e., rinsing, transferring, and crushing) and oxidation (conversion from organic N to nitrate) of "tissue" samples (i.e., foraminifer shells with cytoplasm). Each protocol is described in detail in the supporting information (Text S1). While the resulting $\delta^{15}N$ values were similar between protocols, the 2017 protocol was found to be the least reliable, yielding the largest standard deviations (for replicate oxidations) and the largest number of incomplete ("failed") oxidations (all of which have been excluded). Below, we describe the 2018 protocol, which was the most successful (yielding the smallest standard deviations and no "failed" oxidations).

"Tissue" specimens were transferred to a 4 mL precombusted Wheaton vial and briefly rinsed with Milli-Q (Ren et al., 2012) inside the vial to loosen detritus and dilute any residual nitrate or formalin. After pipetting off the supernatant liquid under a microscope, samples were dried in a dessicator (with silica gel) for 10–16 hr. Once dry, specimens were crushed open with an ethanol-cleaned spatula to expose the foraminiferal tissue for oxidation. This (nonshell-bound) organic N was converted to nitrate by a 1 mL addition of a basic persulfate oxidizing reagent (POR; 1 g potassium persulfate and 0.7 g sodium hydroxide dissolved in 100 mL Milli-Q) and autoclaving on a slow vent setting for 65 min (Knapp et al., 2005; Nydahl, 1978). Blanks (containing POR only) and standards (containing POR plus an amino acid reference material) were included in every batch to correct for the POR-associated N blank and to ensure complete oxidation. At the MPIC, USGS-40 and USGS-41 were used as references (Qi et al., 2003). Analyses carried out at Princeton included (in addition to USGS-40 and/or USGS-41) an in-house mixed alanine-glycine amino acid standard calibrated by analysis with elemental analyzer-isotope ratio mass spectrometry.

"Shell" specimens were cleaned using the same persulfate oxidation method described above (Knapp et al., 2005; Nydahl, 1978), but scaling up the POR recipe (to 2 g potassium persulfate and 2 g sodium hydroxide in 100 mL Milli-Q) and volume addition (to 3 mL) to match the larger number of individuals. After removing the high-nitrate supernatant (from oxidation of the tissue fraction), the crushed shell material was rinsed 6 times with Milli-Q and oven dried at 50 °C. Shell-bound N was released by dissolution of calcite with a 50 μL addition of 4 N hydrochloric acid (HCl), and oxidized to nitrate by a 1 mL addition of POR (in this case, 0.7 g potassium persulfate and 1 g sodium hydroxide dissolved in 100 mL Milli-Q; a more basic recipe to compensate for the HCl addition). Most (~80%) of the shell-bound N measurements were obtained by combining the POR-cleaned shell material (from the same species and tow, or occasionally neighboring tows) leftover from tissue oxidations.

Auxiliary data were obtained from morphometric analysis (using an Olympus SZX16 incident light microscope (planapochromatic), and an Olympus UC90 camera with a resolution of 1.32×1.32 μm per pixel) and weighing (using a Mettler Toledo XP6U comparator 7-digit microbalance). Due to the time required for these steps and the risks of contamination and sample loss (particularly for cleaned shell samples), these measurements were undertaken on only a selection of (mostly tissue) specimens (approximately 14% of all ($n = 1{,}039$) samples measured).

2.3. N Isotope Analyses

All nitrate samples resulting from tissue and shell-bound N oxidation were adjusted to a pH of 5–7 using HCl and measured for nitrate concentration by chemiluminescence (Braman & Hendrix, 1989). Nitrate was quantitatively converted to nitrous oxide (N_2O) using the denitrifier method (Sigman et al., 2001), followed by gas chromatography-isotope ratio mass spectrometry (GC-IRMS; using a Thermo MAT 253 with online N_2O extraction and purification;Casciotti et al., 2002 ; Sigman et al., 2001 ; Weigand et al., 2016). The $\delta^{15}N$ measurements were referenced to N_2 in air using nitrate reference materials USGS-34 and IAEA-NO3. Oxidized samples were corrected for the POR blank (on average, 2% and 5% of the total N in

tissue and shell samples, respectively) using the measured $\delta^{15}N$ and N content of the blanks associated with each batch and calibrated using the amino acid standards. The pooled standard deviations (1σ) of all foraminifer tissue $\delta^{15}N$ and shell-bound $\delta^{15}N$ cleaning-and-oxidation replicates were 1.0‰ ($n = 77$) and 1.2‰ ($n = 14$), respectively, if the 2017 analyses are included, or 0.5‰ ($n = 47$) and 0.8‰ ($n = 6$), respectively, if the 2017 analyses are excluded.

Seawater nitrate samples collected from the Niskin bottles and underway intake were treated with sulfamic acid to remove nitrite (Granger & Sigman, 2009). Nitrate and nitrate+nitrite concentrations were then measured by chemiluminescence (Braman & Hendrix, 1989), and the $\delta^{15}N$ of nitrate and nitrate+nitrite determined using the denitrifier method in conjunction with GC-IRMS (Casciotti et al., 2002; Sigman et al., 2001; Weigand et al., 2016) as described above. The pooled standard deviations (1σ) of seawater nitrate +nitrite $\delta^{15}N$ and nitrate-only $\delta^{15}N$ denitrifier replicates were 0.09‰ and 0.06‰, respectively. For brevity, we focus our attention on the nitrate+nitrite data, which are suggested to be the more "stable" pool (i.e., robust to potential nitrate-nitrite interconversion; Kemeny et al., 2016) and thus possibly a better reflection of the pool available for assimilation by phytoplankton in the Southern Ocean (Fripiat et al., 2019). Regardless, our conclusions are unaffected by the choice of nitrate-only or nitrate+nitrite. Bulk and size-fractionated PON samples were analyzed for $\delta^{15}N$ by elemental analyzer-IRMS (Thermo Scientific FLASH 2000 elemental analyzer coupled to a Thermo Scientific Delta V Plus mass spectrometer) and referenced to atmospheric N_2 using three in-house organic standards (Choc, Merck Gel, and Valine). The pooled standard deviation of replicate analyses was 0.3‰ for bulk and 0.9‰ for size-fractionated samples.

2.4. Species and Size Distributions of Foraminifera: Estimations and Assumptions

It should be noted that the number of foraminifer specimens picked may not accurately represent the abundance of foraminifera in the ocean at the time of sampling. The heterogeneous nature of the tow-collected material (particularly the tendency of some specimens, often small and/or spinose ones, to clump together with algal material and/or detritus) hindered representative subsampling for exact species counts. However, all tow collections underwent the same sieving and density separation procedures and should, thus, be intercomparable (i.e., all being subject to the same potential biases). We therefore do not rely on absolute abundances (i.e., number of individuals of a particular species or size fraction; Figure 2a), but rather focus on the relative abundances (as a percentage of the total foraminifera picked; Figure 2b).

In addition, we consider the first two sets of analyses (2016 and 2017) to more closely resemble the relative species and size proportions within the original tow collection, as foraminifera were picked at random before sorting by species and size. For the last set of analyses (2018), some tows and species were specifically targeted for reanalysis, and their inclusion in the abundance data set (Figure 2) would artificially elevate their contributions; we, therefore, exclude these from the abundance data set. We do, however, draw on detailed morphometric data obtained during the 2018 set of analyses (Text S2 and Figure S1) to test the robustness of observations from the cruder size data (only 3 to 4 size fractions) obtained from visually separating specimens using a microscope reticle (i.e., the only size data available for the 2016 and 2017 analyses).

2.5. Statistical Analysis

To address our prediction that foraminifer $\delta^{15}N$ should vary with nitrate+nitrite $\delta^{15}N$ we use linear mixed effects models (LMMs) to test for a statistically significant relationship between these two variables. LMMs are commonly used to model relationships between a response variable (here, foraminifer $\delta^{15}N$ from tissue or shells) and covariates of interest fit as "fixed effects" (e.g., nitrate+nitrite $\delta^{15}N$) in the presence of a hierarchical (grouped) structure in the data (which is incorporated into the model's "random effects"; Pinheiro & Bates, 2000). Prior to statistical analysis, foraminifer $\delta^{15}N$ data are averaged across replicate ($n = 1$–3) "denitrifier" (isotope) measurements. To account for the nonindependence of samples collected from the same species or from the same site, species (up to $n = 9$) and tow site (up to $n = 14$, depending on the data subset) are fit as crossed random intercepts in all models. In the Southern Ocean, nitrate+nitrite $\delta^{15}N$ varies seasonally; thus, we first evaluate the effect of season (a two-level factor; winter vs. late summer) on foraminifer $\delta^{15}N$ using combined data from both cruises (season is fit as the sole fixed effect predictor of foraminifer $\delta^{15}N$; species and tow site are included as random effects; Table S4). We then divide the data by cruise and estimate the relationship between nitrate+nitrite $\delta^{15}N$ (again, fit as the only fixed-effect predictor) and foraminifer $\delta^{15}N$ separately for samples collected in winter versus late summer. Latitude, bulk PON $\delta^{15}N$, and

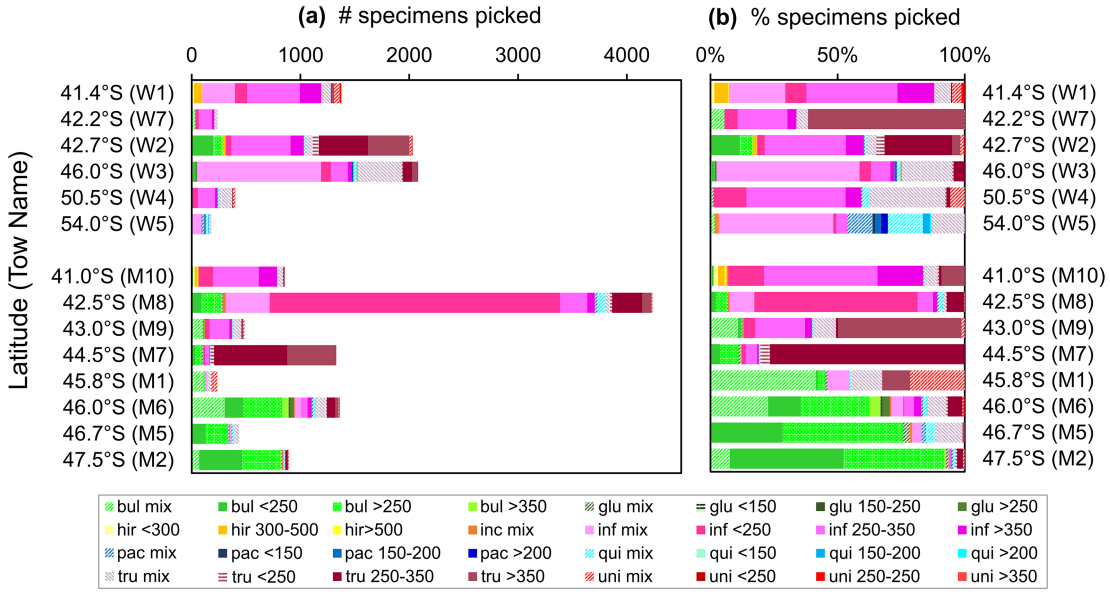

Figure 2. The (a) absolute and (b) relative abundances of foraminifera specimens picked from net tow collections in winter 2015 (top set; indicated by "W") and late summer 2016 (bottom set; indicated by "M"). Colors represent different foraminifer species, with variations in hue and texture indicating different size fractions (as per the figure legend, in μm). Only the results of the 2016 and 2017 analyses are shown here (as our most representative subset of the original collections) where size fractions were separated by eye using a microscope reticle. Morphometric measurements made during the 2018 analyses are shown in Figure S1 in the supporting information. The legend label "mix" indicates a sample of mixed specimen size, where there were not enough individuals for size-fractionated N measurements.

zooplankton $\delta^{15}N$ are also evaluated as environmental predictors of foraminifer $\delta^{15}N$ in single-fixed-effect models run on the season-separated data. Coefficient estimates, standard errors and p values describing these relationships are presented in Tables S5 and S6 for winter and late summer, respectively. This first stage of statistical analysis estimates the overall effects (i.e., across species and tow sites) of our covariates of interest (nitrate+nitrite $\delta^{15}N$, season, latitude, bulk PON $\delta^{15}N$, and zooplankton $\delta^{15}N$). In the second stage of analysis, we evaluate species-specific responses to the four environmental predictors using data from the five most abundant species in each season (those sampled ≥5 times). In Stage 2, variation in foraminifer $\delta^{15}N$ is modeled as a function of species (a multilevel factor), one of the environmental predictors, and the species × environment interaction (describing the degree to which, e.g., nitrate+nitrite $\delta^{15}N$ effects on foraminifer $\delta^{15}N$ were species-specific). As in Stage 1, Stage 2 models quantifying species-specific effects of season include data from both cruises; analyses are separated by cruise/season for all other environmental variables. In Stage 2 models, tow site is fit as a random effect. Species-specific slope estimates, standard errors, and p values are presented in Tables S7 and S8. All LMMs were run in MATLAB (R2019a). Throughout this paper we combine a presentation of the raw data (describing patterns; relevant to comparisons with other studies) with statistical inferences from the LMMs (providing an appropriate test of the relationships of interest). R^2 values presented for the LMMs include the variance explained by both fixed and random effects (Nakagawa & Schielzeth, 2013).

To assess the effect of season, separate statistical analyses are run using foraminifer tissue $\delta^{15}N$ ($n = 245$) as the response variable and with shell-bound $\delta^{15}N$ ($n = 50$) as the response variable. Statistical analyses are also repeated using a data set that excludes tow sites W5 and M10 ($n = 220$ for tissue; $n = 46$ for shell), which fall outside of the core SAZ/PFZ, and using a data set additionally excluding samples processed in 2017 ($n = 133$ for tissue; $n = 20$ for shell). Coefficient estimates, standard error, and p values are presented in Table S4. Results are very similar for shell and tissue $\delta^{15}N$ samples and are unchanged when excluding data from tow sites W5 and M10 or from the 2017 processing. We take this, plus a strong positive covariation between foraminifer tissue $\delta^{15}N$ and shell $\delta^{15}N$ using all available data pairs from replicate oxidations (discussed below), as justification for analyzing the effects of the other environmental predictors (not season) on tissue $\delta^{15}N$ samples only (from the core SAZ/PFZ, including those processed in 2017).

3. Results

3.1. Hydrographic and Nitrate+Nitrite Conditions

During the winter 2015 voyage (Figure 1a), the subsurface core of the STF was located at 40.7°S with its surface expression between 39.7°S and 40.9°S. The SAF, the PF, and the Southern Antarctic Circumpolar Current Front were located at 43.8°S, 50.6°S, and 55.7°S, respectively. Along the late-summer 2016 transect (Figure 1b), the core of the Agulhas Current was located at ~36–38°S, and the Agulhas Retroflection was encountered at ~38–41°S. The northern (N-STF) branch of the STF was near 41.0°S, while the southern branch (S-STF) was at around 41.5°S. The SAF was divided into a northern (N-SAF; ~42.5°S), middle (M-SAF; ~45.8°S) and southern (S-SAF; ~46.8°S) branch. The PF was located well south of Marion Island at ~50.5°S at the time of sampling. Mixed-layer depth was 110–147 m at the winter tow stations and 92–107 m in late summer at all but station M10 where it was shallower than 60 m. Comparing only the SAZ/PFZ stations (i.e., excluding the southernmost winter tow W5 and the northernmost summer tow M10), mixed layers were ~30 m deeper on average for the winter 2015 transect. Mixed-layer fluorescence, a proxy for chlorophyll concentration, was lower in winter (0.4–0.8 mg/m^3) than in late summer (0.7–1.8 mg/m^3), generally increasing equatorward and peaking in the northern SAZ (not shown).

In the Open Antarctic Zone (OAZ), nitrate-rich Upper Circumpolar Deep Water (UCDW) upwells year-round (due to Ekman divergence; Nowlin & Klinck, 1986, and references therein) through the base of the winter mixed layer (which underlies a shallower mixed layer during summer) and is incorporated into surface waters by the homogenization of the two (former summer and winter) mixed layers during wintertime cooling and mixed-layer deepening (Sigman, Altabet, McCorkle, et al., 1999; Toole, 1981). Both the PFZ and SAZ mixed layers are supplied laterally by equatorward Ekman transport (of nitrate from the adjacent polar mixed layer) and vertically by mixing with the underlying thermocline (DiFiore et al., 2006; McCartney, 1977; Sigman, Altabet, McCorkle, et al., 1999). From south to north along the winter transect, mixed-layer nitrate+nitrite concentrations (triangles in Figure 3a) decrease from ~29 μM at the southernmost station located in the OAZ, to 18–27 μM at the PFZ stations, to 6–17 μM in the SAZ, and remain between 6 and 7 μM north of the STF. Over the same area, nitrate+nitrite δ^{15}N (triangles in Figure 3b) increases from ~5.4‰ in the OAZ to ~6.0–7.5‰ in the PFZ to 7.7–11.4‰ in the SAZ and then decreases to ~9.5‰ into the STZ. Along the late-summer transect, surface nitrate+nitrite concentrations (circles in Figure 3a) decrease from 20–23 μM in the PFZ (the southernmost stations on the voyage), to 13–20 μM in the SAZ, to 5–7 μM just north of the STF in the Agulhas Retroflection (MT10 in Figure 1b). Over the same area, nitrate+nitrite δ^{15}N (circles in Figure 3b) increases from ~7.0–7.5‰ in the PFZ to ~7.8–9.8‰ in the SAZ before decreasing to ~8.4‰ at the northernmost station. In both the winter and late summer profiles, the nitrate+nitrite concentration decreases upwards through the water column from the subsurface maximum of UCDW (which shoals poleward from ~1,100–1,500 m in the SAZ to ~200 m in the OAZ, along the 1,027.6 kg/m^3 isopycnal), and reaches minimum values within the surface mixed layer. This trend is qualitatively mirrored by nitrate+nitrite δ^{15}N, which increases from deep to shallow, particularly through the thermocline (between ~200 and 100 m). The magnitude of the deep-to-shallow changes in nitrate+nitrite concentration and δ^{15}N generally increases with decreasing latitude, except north of the STF. Nitrate-only concentration and δ^{15}N (from seawater samples with nitrite removed; dotted profiles in Figure S2) exhibit similar patterns to nitrate+nitrite (described above), but generally have higher δ^{15}N values (typically by ~0.3–1.0‰) in the mixed layer.

The average nitrate+nitrite concentration and δ^{15}N of UCDW (identified by its characteristic potential density (~1,027.6 kg/m^3) and low oxygen content (~3.7 mL/L); not shown) on the winter transect are 36.5 ± 1.4 μM and 5.1 ± 0.2‰ (n = 5), respectively, compared to 34.7 ± 0.9 μM and 5.2 ± 0.1‰ (n = 6) on the late-summer transect. Using only data from the core of the SAZ/PFZ yields a slightly different nitrate+nitrite concentration and δ^{15}N for winter UCDW (36.9 ± 0.9 μM and 5.2 ± 0.1‰ (n = 2), respectively), but makes no difference to the late-summer values. In either case, UCDW nitrate+nitrite is significantly different between the transects in terms of concentration ($p < 0.05$), but not in terms of δ^{15}N ($p > 0.05$ based on a two-sample, equal variances t test). AAIW is identified by pronounced subsurface salinity minima (<34.3 psu) and weak local oxygen maxima (~5 mL/L) north of the SAF (not shown) and is roughly bounded by the 1,027.05 and 1,027.4 kg/m^3 isopycnals. The average nitrate+nitrite concentration and δ^{15}N of AAIW are 29.1 ± 1.0 μM (n = 2) and 5.9 ± 0.1‰ (n = 2), respectively, for the winter transect and 29.8 ± 2.4 μM

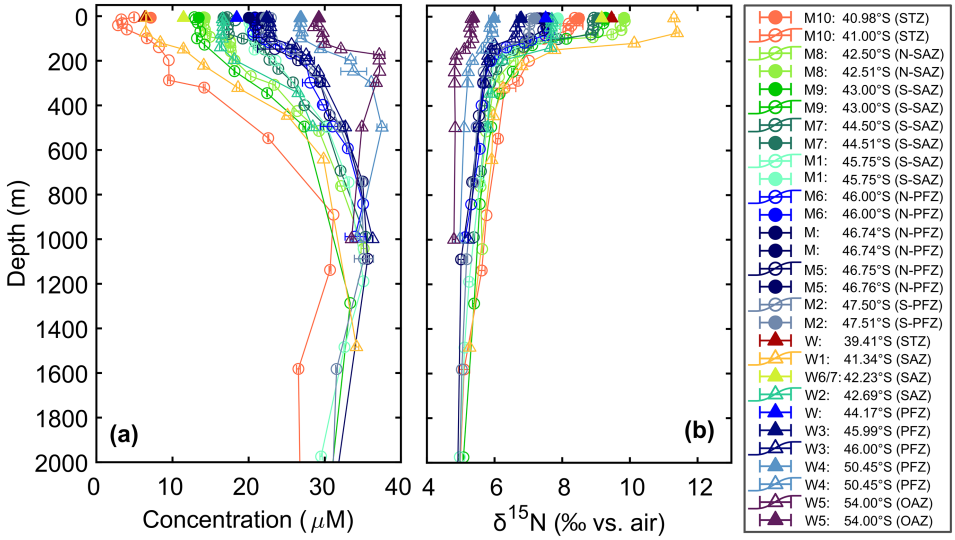

Figure 3. Depth profiles (open symbols) and surface (filled symbols) measurements of nitrate+nitrite (a) concentration (in μM), and (b) $\delta^{15}N$ (in ‰ vs. N_2 in air) for the upper 2,000 m from the winter (triangles) and late summer (circles) transects south of Africa. Data are colored by latitudinal zone, with the Subtropical Zone (STZ) and Subtropical Front (STF) shown in warm colors, the Subantarctic Zone (SAZ) in green, the Polar Frontal Zone (PFZ) in blue and the Open Antarctic Zone (OAZ) in purple. Legend labels give the associated tow name where applicable (or cruise code (M or W) where no tow was performed), followed by the latitude and zone of the depth profile. Error bars indicate the measurement standard deviation ($n \geq 2$). For a comparison with nitrate-only (i.e., after nitrite removal; see section 2), refer to Figure S2 in the supporting information.

($n = 9$) and 5.7 ± 0.1‰ ($n = 10$), respectively, for the late-summer transect. Neither concentration nor $\delta^{15}N$ differences in AAIW between cruises are significant ($p > 0.05$). Directly beneath the SAZ mixed layer and above AAIW lies SAMW, identified by its high salinity (>34.3 psu) and relatively low oxygen content in a density range of approximately 1,026.7–1,027.05 kg/m^3. The average nitrate+nitrite concentration and $\delta^{15}N$ of SAMW on the winter transect are 20.5 ± 5.2 μM and 6.2 ± 0.4‰ ($n = 5$), respectively, not significantly different from 21.6 ± 2.6 μM and 6.3 ± 0.3 ($n = 12$) on the late-summer transect ($p \gg 0.05$). The average nitrate+nitrite concentration and $\delta^{15}N$ given here for UCDW, AAIW, and SAMW are typically within 1–3 μM and 0.0–0.4‰, respectively, of those reported previously for the Atlantic (Smart et al. (2015)), and Indo-Pacific sectors (Sigman et al., 2000; Rafter et al., 2012,); Rafter et al., 2013).

Combining data from only the SAZ and PFZ stations shows that the late-summer mixed layer (with $n = 44$ samples) has a lower nitrate+nitrite concentration (19.1 ± 3.4 μM) and higher nitrate+nitrite $\delta^{15}N$ (8.1 ± 0.9‰) than the winter mixed layer (20.0 ± 6.5 μM and 7.3 ± 1.6‰, respectively; with $n = 18$). The $\delta^{15}N$ difference is significant ($p < 0.05$), but the concentration difference is not ($p > 0.05$). Mixed-layer nitrate-only (dotted profiles in Figure S2) at the same stations has higher $\delta^{15}N$ values than nitrate+nitrite (solid profiles in Figure S2), by 0.4 ± 0.2‰ ($n = 18$; $p > 0.05$, i.e., not significantly higher) for winter and by 0.8 ± 0.1‰ ($n = 44$; $p \ll 0.05$, i.e., significantly higher) for late summer on average, implying low $\delta^{15}N$ values for mixed-layer nitrite of −10 ± 11‰ ($n = 18$) and −34 ± 25‰ ($n = 36$) for winter and late summer, respectively, based on mass balance calculations. The lowest mixed-layer nitrite $\delta^{15}N$ values are calculated for the late summer PFZ (−50 ± 28‰; $n = 15$), significantly lower than for the winter PFZ (−7 ± 6‰; $n = 9$). Within the SAZ, mixed-layer nitrite $\delta^{15}N$ is also lower in late summer (−22 ± 15‰; $n = 21$) than in winter (−14 ± 15‰; $n = 8$), although this difference is not significant.

3.2. Species and Size Distributions of Foraminifera and Other Zooplankton

Based on microscope observations made ship-board, the smallest net tow size-fraction (<150 μm) consisted mostly of detritus, with very few foraminifera. Foraminifera were most common in the 150–250 μm and 250–500 μm size fractions, which also contained small crustaceans (mostly amphipods, isopods and ostracods) and, in some tows, pteropods (pelagic sea snails). Intermediate size fractions (500–1,000 μm and 1,000–2,000 μm) were dominated by crustaceans (including krill, amphipods, copepods, and ostracods),

pteropods, and fish larvae. The largest size fractions (2,000–5,000 μm and >5,000 μm) were typically dominated by gelatinous species (including salps and chaetognaths), and/or larger crustaceans, with the occasional fish or fish larvae.

On average, late-summer tows yielded double the number of foraminifer specimens obtained from winter tows (Figure 2a). Winter assemblages contain primarily *G. inflata* and *G. truncatulinoides* (averaging 60% and 20% of the total picked foraminifera, respectively), while late-summer assemblages are dominated by *G. bulloides*, *G. inflata*, and/or *G. truncatulinoides* (averaging 40%, 30%, and 20%, respectively; Figures 2a and 2b). Near the STF, the total abundance and species compositions of foraminifera are similar in winter (W1) and late summer (M10), with *G. inflata* contributing 80–90% and *G. hirsuta* contributing 6–8%. *O. universa* is present at low abundances (<3%) in most summertime collections and some winter tows, with peak abundances (24%) at station M1 (45.8°S) near the M-SAF. *G. glutinata* generally occurs in low numbers but appears more commonly in tows where *G. bulloides* dominates the assemblage. *N. incompta* is present in most summer and some winter tows, but typically makes up <2% of the total assemblage. *N. pachyderma* and *T. quinqueloba* are generally scarce, only contributing substantially (12% and 16%, respectively) to the total foraminifer assemblage in the southernmost winter tow, in the OAZ.

Foraminifera were particularly abundant at late-summer station M8 (42.5°S; near the N-SAF, where peak chlorophyll concentrations (not shown) of ~1.8 mg/m^3 were observed; Figure 2a). The population was dominated by small (<250 μm) *G. inflata*, in contrast with the larger 250–350-μm-dominated size distribution of *G. inflata* in every other tow collection (Figure 2b).

3.3. δ^{15}N of Bulk and Size-Fractionated Particulate Organic N

The δ^{15}N of bulk PON collected in surface waters (gray filled diamonds in Figures 4a and 4b) is significantly ($p \ll 0.05$) higher for the winter transect (2.8 ± 0.3‰, $n = 26$) than for the late-summer transect (0.4 ± 0.5‰, $n = 25$). Considering only the core of the SAZ/PFZ (excluding data that fall in the shaded margins of Figure 4), the difference between cruises is even larger, with PON δ^{15}N averaging 3.2 ± 0.7‰ ($n = 9$) and − 2.0 ± 0.4‰ ($n = 12$), respectively. Bulk PON δ^{15}N rises by ~7‰ from south-to-north across the entire late-summer transect (from 47.5°S to 35.5°S), ~4‰ of which occurs across the SAZ/PFZ. In winter, the trend in bulk PON δ^{15}N (between 55.7°S and 34.5°S) is not linear: increasing from the AZ to PFZ, decreasing across the PFZ and SAZ (by ~5‰), and then increasing again into the subtropics.

Similarly, the δ^{15}N of size-fractionated tow material increases from south-to-north in late summer but not in winter, with significantly ($p \ll 0.05$) higher values in winter (4.7 ± 0.2‰; $n = 42$; Figure 4c) than in late summer (1.1 ± 0.3‰; $n = 54$; Figure 4d). Excluding data outside of the core SAZ/PFZ yields similar averages of 4.8 ± 0.2‰ ($n = 36$) for winter and 0.9 ± 0.3‰ ($n = 48$) for late summer (also with $p \ll 0.05$). In both cases, size-fractionated tow material is generally higher in δ^{15}N than surface-ocean bulk PON from the same site (by 2.6 ± 0.4‰ ($n = 12$) for all tows with both measurements; by 2.9 ± 0.4‰ ($n = 10$) for the SAZ/PFZ tows). The significant difference between winter and late summer applies to the bulk tow material (i.e., combining all size fractions from <150 to 5,000 μm) as well as to each individual size fraction. We exclude the >5,000 μm fraction from the comparison, as it was only collected on the late-summer cruise. On average, there is a δ^{15}N increase from smaller (150–250 μm or 250–500 μm) to larger (2,000–5,000 μm) size fractions in both seasons (although this trend is less consistent for the winter tows), with a larger range of values in late summer (from −0.8 ± 0.8‰ ($n = 7$) to 1.9 ± 0.6‰ ($n = 12$), respectively) than in winter (from 4.4 ± 0.3‰ ($n = 6$) to 5.1 ± 0.4‰ ($n = 8$), respectively). A notable exception is the smallest size fraction (<150 μm), which has a high δ^{15}N that is comparable to the medium-to-large size fractions from the same tow.

3.4. δ^{15}N of Foraminifera

3.4.1. Tissue and Shell-Bound N

As observed for bulk and size-fractionated PON, the δ^{15}N of foraminifer tissue is significantly higher (by 3.9 ± 0.8‰) in the winter (4.5 ± 0.7‰; all circles in Figure 4e) than in the late summer (0.6 ± 0.6‰; all circles in Figure 4f) tow collections ($n = 308$; $p \ll 0.05$ based on a LMM predicting foraminifer δ^{15}N by season; Table S4a). The δ^{15}N of foraminifer shells (triangles in Figures 4g and 4h) is more variable (within and among species) than that of tissue samples, but shows the same tendencies described above. Shell-bound δ^{15}N is significantly higher (by 3.9 ± 1.5‰ with $p < 0.05$; $n = 69$; Table S4d) in winter (5.7 ± 1.3‰) than in late summer (1.8 ± 1.1‰). Undertaking the same comparison for SAZ/PFZ tows only (excluding tows near the STF [M10]

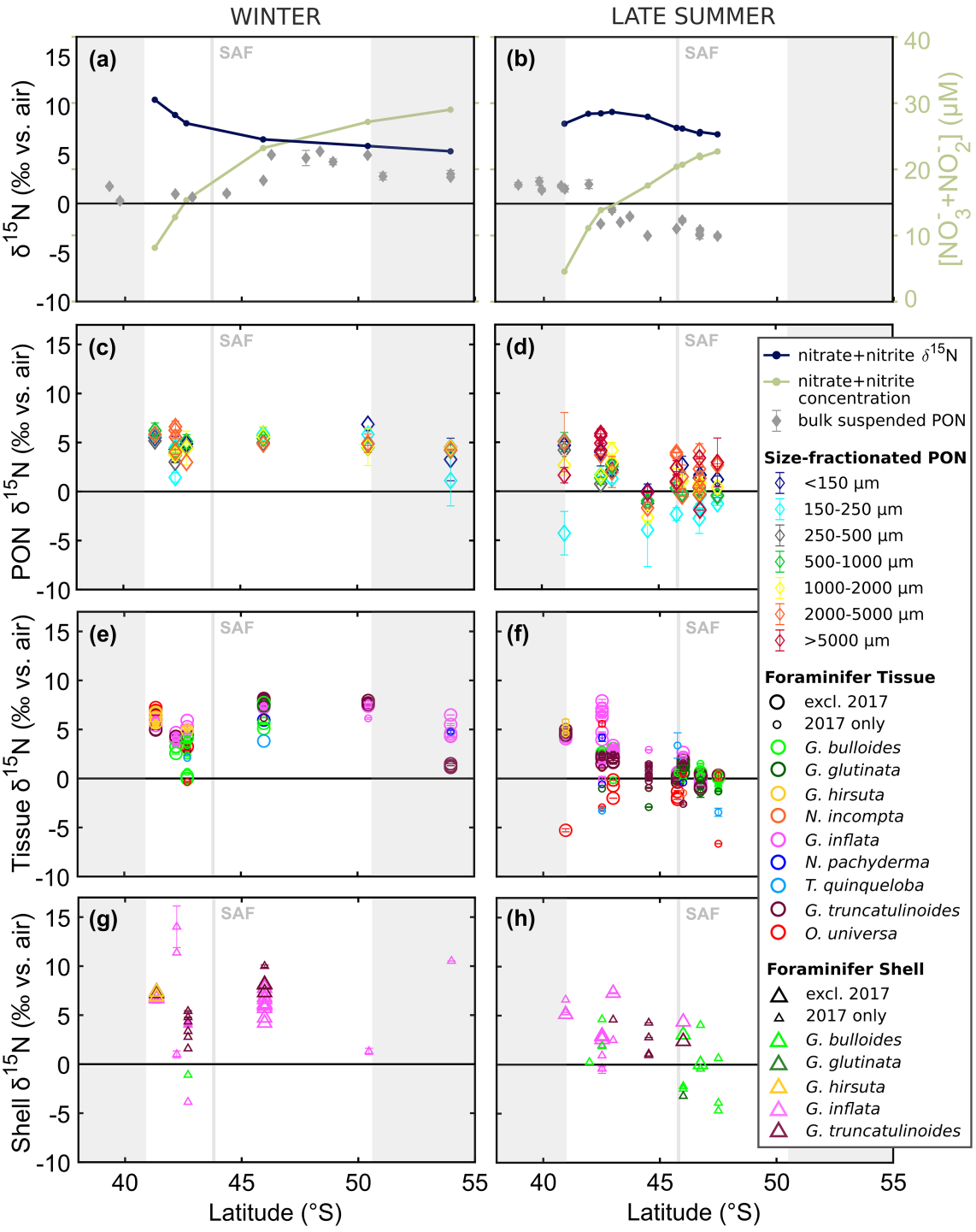

Figure 4. Top panels show in situ (i.e., tow depth) nitrate+nitrite concentration (light green line; secondary *y* axis) and $\delta^{15}N$ (dark blue line; primary *y* axis) along the (a) winter and (b) late-summer transects, as well as surface-water bulk (>0.7 μm) suspended PON $\delta^{15}N$ (filled, gray diamonds). The second row of panels show transects of size-fractionated PON $\delta^{15}N$ (open, colored diamonds) from the same net tows, during (c) winter and (d) late summer, where each color represents a different size fraction (from <150 μm to >5,000 μm). The four lower panels show transects of foraminifer tissue (circles; e and f) and shell (triangles; g and h) $\delta^{15}N$ from mixed-layer net tow collections during (e and g) winter and (f and h) late summer, where each color represents a different foraminifer species. The 2017 analyses are denoted by small symbols (circles and triangles), for comparison with the combined 2016 and 2018 analyses (large symbols, where 2017 analyses are excluded from sample averages). Light gray-shaded areas fall outside of the core PFZ/SAZ (the focus of this study), and the vertical gray line denotes the latitude of the Subantarctic Front (SAF), which divides the PFZ and the SAZ. Error bars indicate the standard deviation of replicate isotope measurements (typically $n = 2$–3).

and those south of the PF [W5]), yields the same key results: The $\delta^{15}N$ of foraminifer tissue is significantly higher (by 4.6 ± 0.8‰) in the winter (4.8 ± 0.7‰) than in the late summer (0.2 ± 0.6‰) tow collections ($p \ll 0.05$; $n = 283$; Table S4b). In general, foraminifer tissue is higher in $\delta^{15}N$ than surface-ocean bulk PON (by 2.9 ± 0.3‰ ($n = 12$) for all tows with both measurements; by 3.2 ± 0.2‰ ($n = 10$) for the SAZ/PFZ tows; Table 2), but similar in $\delta^{15}N$ to size-fractionated tow material (higher by 0.2 ± 1.1‰ ($n = 14$) for all tows; higher by 0.2 ± 1.2‰ ($n = 12$) for the SAZ/PFZ tows) from the same site. The late-summer-versus-winter difference in foraminifer tissue $\delta^{15}N$ is significant ($p < 0.05$) in all seven of the species for which we have tissue data from both seasons (i.e., all except *G. glutinata* and *G. hirsuta*; model coefficients not shown).

Late-summer tissue $\delta^{15}N$ exhibits a south-to-north increase by ~3.1‰ (Figure 4f), while the winter trend shows the opposite: a ~2.9‰ decrease across the SAZ/PFZ (Figure 4e). Excluding the 2017 analyses raises winter and summer tissue $\delta^{15}N$ slightly to 5.3 ± 0.8‰ and 0.8 ± 0.7‰, respectively, but has little effect on the magnitude of late-summer-versus-winter difference (4.5 ± 0.9‰ instead of 4.6 ± 0.8‰) or its significance ($p \ll 0.05$; $n = 168$; Table S4c). The effect on latitudinal changes (from south to north) is to strengthen the late-summer trend (to a 4.3‰ rise) but weaken the winter trend (to a 2.4‰ decline) across the SAZ/PFZ. We explore these trends further in section 3.4.2 below. The $\delta^{15}N$ of foraminifer shells is still more variable than tissue (within and among species) in the SAZ/PFZ, but generally shows the same tendencies described for SAZ/PFZ tissue $\delta^{15}N$. Again, shell-bound $\delta^{15}N$ is significantly higher (by 4.0 ± 1.5‰ with $p < 0.05$; $n = 65$; Table S4e) in winter (5.3 ± 1.2‰) than in late summer (1.3 ± 1.1‰). At the species level, the late-summer-versus-winter difference in shell $\delta^{15}N$ is only significant ($p < 0.05$) for *G. truncatulinoides* (one of the three species with shell data from both seasons; not shown). Excluding the 2017 analyses raises the winter and summer shell $\delta^{15}N$ averages (to 6.8 ± 1.7‰ and 3.5 ± 1.3‰, respectively), thereby reducing the late-summer-versus-winter difference (to 3.3 ± 2.1‰ instead of 4.0 ± 1.5‰), which is no longer significant ($p > 0.05$; $n = 28$; Table S4f). An overview of the foraminifer tissue and shell-bound $\delta^{15}N$ by species is presented in Table 1. For summaries of the N content of foraminifer tissue and shells, refer to the supporting information (Tables S2 and S3).

There is a strong ($R^2 = 0.9$) and significant ($p < 0.05$) positive relationship between foraminifer tissue and shell-bound $\delta^{15}N$ with a slope of 0.8 (dashed black line in Figure 5), based on all available data pairs ($n = 33$; i.e., where tissue and shell measurements were made of the same species, from the same net tow, but not necessarily of the same individuals). While the individual species data appear roughly consistent with this overall trend (especially for *G. truncatulinoides*), the small sample sizes prevent us from evaluating them explicitly. The intermediate-dwelling *G. bulloides* (and possibly *G. glutinata*) cluster at lower $\delta^{15}N$ (typically <2‰), while deeper-dwelling *G. inflata*, *G. truncatulinoides*, and *G. hirsuta* span a higher $\delta^{15}N$ range (typically >2‰). Using all data pairs from both transects, the average $\delta^{15}N$ of foraminifera is 3.4 ± 0.7‰ for tissue and 3.0 ± 1.4‰ for shells ($n = 33$).

3.4.2. Trends in Foraminifer Tissue $\delta^{15}N$ With Latitude, Nitrate+Nitrite $\delta^{15}N$ and PON $\delta^{15}N$

Below, we focus on trends in foraminifer tissue $\delta^{15}N$ (rather than shell-bound $\delta^{15}N$, as these data are sparse and more variable) within the SAZ/PFZ. Given that excluding the 2017 lab analyses has no effect on our findings, we include these data to increase sample size. In late summer, foraminifer tissue $\delta^{15}N$ shows a significant northward increase overall (i.e., negative slope and $p \ll 0.05$), with a slope of −0.5 (Figure 6e; Table S6a). This trend is evident and significant in four of the five species with sufficient data to test (*G. bulloides*, *G. inflata*, *G. truncatulinoides*, and *O. universa*; Table S7). *G. glutinata*, on the other hand, exhibits a weak, nonsignificant, southward increases in $\delta^{15}N$ in late summer (i.e., small positive slope with $p \gg 0.05$). In winter, the relationship between foraminifer tissue $\delta^{15}N$ and latitude is reversed, with a weak, nonsignificant northward decrease (i.e., positive slope of 0.3 and $p > 0.05$; Figure 6a; Table S5a). Considering each species (those with sufficient samples) separately produces a range of (positive and negative) slopes (Table S8), largely depending on the latitudinal distribution of the species, with a local minimum in tissue $\delta^{15}N$ at W7 (42.2°S). The relationship between foraminifer tissue $\delta^{15}N$ and in situ nitrate+nitrite $\delta^{15}N$ is positive and significant in late summer (slope = 0.9; $p \ll 0.05$; Figure 6f; Table S6b), but negative and nonsignificant in winter (slope = −0.5; $p > 0.05$; Figure 6b; Table S5b). The species-specific trends generally conform to the overall trends, with mostly positive slopes in late summer (between 0.8 and 1.4; excluding *G. glutinata*; Table S7) and a variety of nonsignificant-positive and -negative slopes in winter (between −1.0 and + 0.4; Table S8).

Table 1
Overview of Tow-Caught Foraminifer Tissue and Shell-Bound $\delta^{15}N$

	Tissue $\delta^{15}N$ (‰)							Shell-bound $\delta^{15}N$ (‰)						
	Late summer			Winter			Winter minus late summer	Late summer			Winter			Winter minus late summer
Species	Mean	SE	*n*	Mean	SE	*n*	diff	Mean	SE	*n*	Mean	SE	*n*	diff
G. bulloides	**0.8**	0.2	25	**3.3**	0.8	5	2.6	**0.3**	0.9	10	**−1.1**	—	1	−1.4
G. inflata	**2.5**	0.4	22	**5.9**	0.3	22	3.4	**2.9**	1.1	6	**4.3**	1.5	9	1.4
G. truncatulinoides	**1.1**	0.2	19	**5.9**	0.6	13	4.8	**2.9**	0.6	4	**6.5**	1.2	5	3.6
O. universa	**−0.8**	0.8	5	**4.3**	1.1	5	5.1	-	—	0	—	—	0	—
G. hirsuta	—	—	0	**5.6**	0.2	7	—	—	—	0	**7.1**	—	1	—
G. glutinata	**−0.7**	0.6	6	**7.4**	—	1	8.1	**−3.2**	—	1	—	—	0	—
N. incompta	**−0.2**	1.3	2	—	—	0	—	—	—	0	—	—	0	—
T. quinqueloba	**−1.1**	2.2	3	**3.0**	0.9	2	4.1	—	—	0	—	—	0	—
N. pachyderma	**0.7**	1.1	2	**6.0**	—	1	5.3	—	—	0	—	—	0	—

Note. $\delta^{15}N$ values are in ‰ versus N_2 in air. Winter and late-summer means (bold), with SE = standard error; *n* = number of oxidations, are shown in separate columns. The simple $\delta^{15}N$ difference (underlined) between the two seasons is given alongside.

In contrast, the $\delta^{15}N$ relationship between mixed-layer foraminifer tissue and bulk surface PON is positive in both winter and late summer, with overall slopes of 0.7 ($p > 0.05$; Figure 6c; Table S5c) and 0.9 ($p \ll 0.05$; Figure 6g; Table S6c), respectively. In late summer, significant species-specific trends (all $p < 0.05$) exist for *G. glutinata* (slope = 1.4), *G. bulloides* (slope = 0.8), *G. inflata* (slope = 0.9), and *G. truncatulinoides* (slope = 0.8; Table S7). A similarly consistent positive relationship is observed between foraminifer $\delta^{15}N$ and tow-caught PON $\delta^{15}N$ (i.e., other zooplankton and larger detritus from the same tows as the foraminifera). Zooplankton $\delta^{15}N$ positively covaries with foraminifer $\delta^{15}N$ in both winter (overall slope = 1.9; $p < 0.05$; Figure 6d; Table S5d) and late summer (overall slope = 0.5; $p < 0.05$; Figure 6h; Table S6d). The zooplankton-foraminifer $\delta^{15}N$ relationship is significant for *G. inflata* in both seasons, as well as for *G. truncatulinoides* and *O. universa* in winter, and for *G. bulloides* in late summer (slopes and *p* values in Tables S7 and S8). The high-$\delta^{15}N$ outliers of *G. inflata* tissue in all late-summer panels (Figures 6e–6h) derive from a

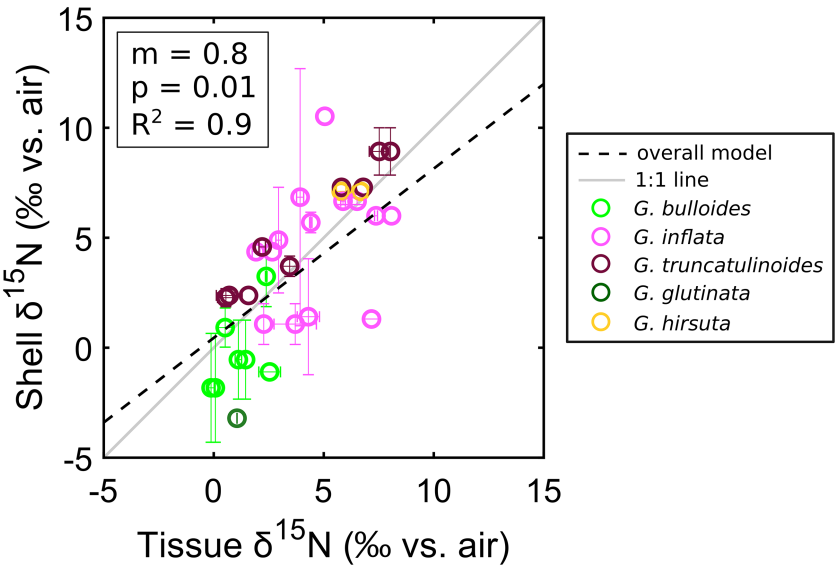

Figure 5. Cross-plot of foraminifer tissue $\delta^{15}N$ versus shell-bound $\delta^{15}N$ for all available data pairs (i.e., measurements of the same species from the same tow collection), with color denoting species. The overall LMM is also plotted (dashed, black line), with a 1:1 line (solid, gray diagonal) included for reference. Error bars indicate the standard error of repeat oxidation measurements of the same species from the same tow.

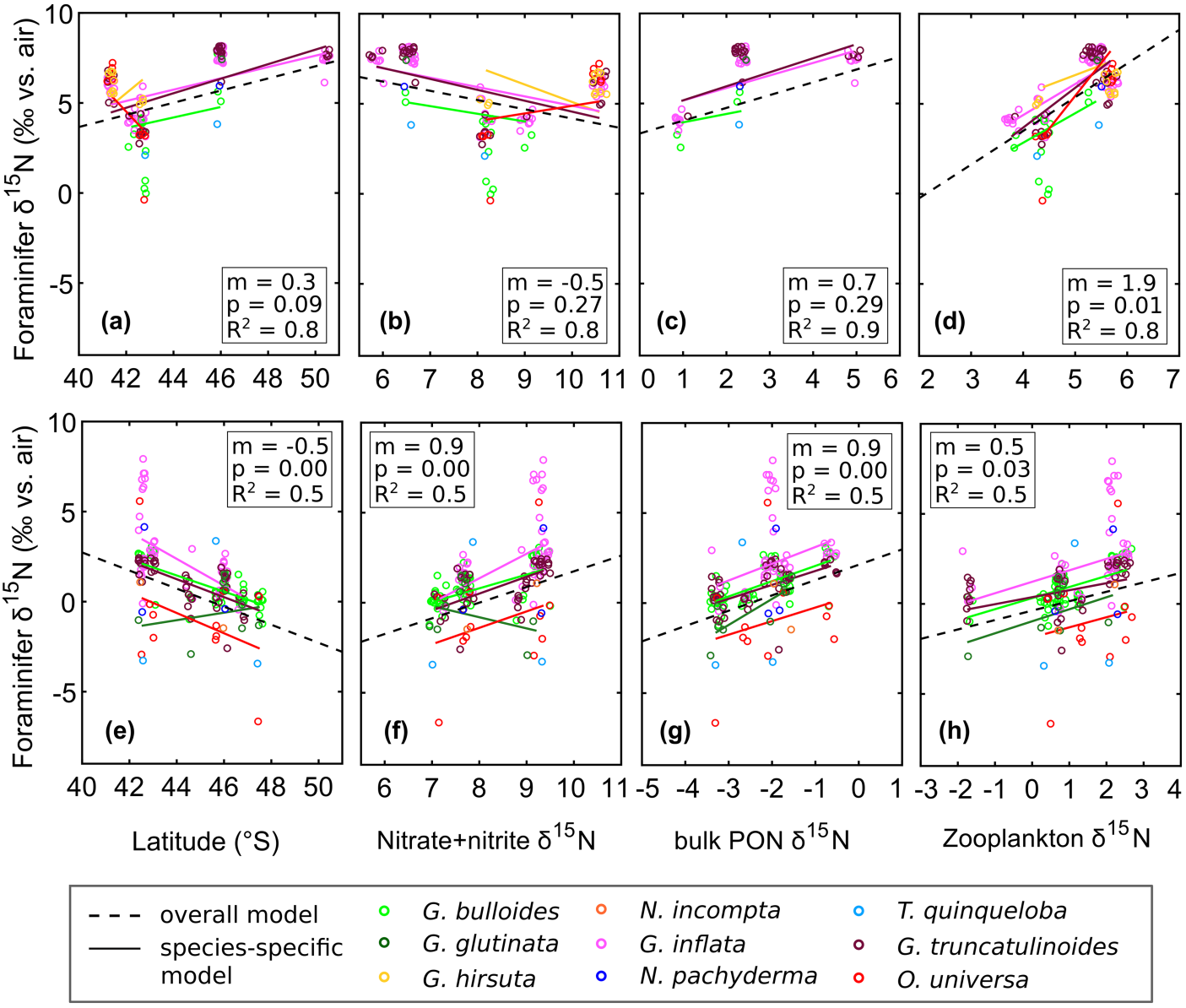

Figure 6. Relationship between foraminifer tissue $\delta^{15}N$ and (a, e) latitude, (b, f) nitrate+nitrite $\delta^{15}N$, (c, g) bulk (>0.7 μm) suspended PON $\delta^{15}N$, and (d, h) zooplankton (i.e., size-fractionated tow PON) $\delta^{15}N$ in the African PFZ/SAZ mixed layer during winter (top row) and late summer (bottom row). LMM lines are drawn for individual species (solid, color lines; those with $n \geq 5$) and overall (dashed, black line). Circles denote the raw data (averaged across replicate (typically $n = 2$) "denitrifier" (isotope) measurements) used in the models, colored by species. For improved visibility, data points are jittered and shown without error bars (which are small for denitrifier replicates; pooled standard deviation of 0.15‰ for tissue $\delta^{15}N$).

single tow station, M8 at 42.5°S. Elevated productivity (evident from the peak in chlorophyll (not shown) and foraminiferal abundance; Figure 2a) and different population dynamics (dominance of small ((<250 μm) *G. inflata*) at M8 might have contributed to the locally high and variable tissue $\delta^{15}N$ of *G. inflata* (e.g., compared to in situ shell-bound $\delta^{15}N$ at the same latitude; compare Figure 4f with Figure 4h at 42.5°S). Rerunning our analyses on data excluding station M8 did not alter our results.

4. Discussion

Given the dominant control of nitrate assimilation on the $\delta^{15}N$ of nitrate+nitrite (hereafter, "nitrate") across the Southern Ocean (Lourey et al., 2003; Sigman, Altabet, McCorkle, et al., 1999), we expected that the $\delta^{15}N$

of surface ocean-dwelling planktic foraminifera would track patterns of $\delta^{15}N$ in nitrate, following the progressive south-to-north and winter-to-summer drawdown of nitrate by phytoplankton. We thus predicted (1) a northward increase in foraminifer $\delta^{15}N$ and (2) higher foraminifer $\delta^{15}N$ values in summer than in winter samples. Following expectations, foraminifer $\delta^{15}N$ increased equatorward in late summer. However, the opposite pattern ($\delta^{15}N$ decreasing equatorward) was observed in winter. Also deviating from our prediction, foraminifer $\delta^{15}N$ was higher in winter than in summer.

Our results show that the $\delta^{15}N$ of foraminifera in the Southern Ocean mixed layer does not simply track the $\delta^{15}N$ of ambient nitrate, at least not year-round. The divergence of foraminifer $\delta^{15}N$ from nitrate $\delta^{15}N$ appears to be related to a similar divergence of upper-water column PON $\delta^{15}N$ from nitrate $\delta^{15}N$. However, in order to best interpret the seasonal and latitudinal patterns in living foraminifer $\delta^{15}N$ and assess their implications for the paleo-proxy, we must first address the contributions of spatial differences (i.e., sampling different regions with potentially different nitrate source properties, N isotope dynamics and/or PON properties) and foraminifer assemblage differences (i.e., the prevalence of different species and/or size fractions) to the apparent "winter versus late summer" differences. Because different latitudinal bands or "zones" of the Southern Ocean are characterized by different hydrodynamic regimes and nitrate sources, and possibly different isotope effects for nitrate assimilation (Altabet & François, 2001; DiFiore et al., 2006; DiFiore et al., 2010; Sigman, Altabet, McCorkle, et al., 1999), we focus our analysis on the zones where the two cruises overlap: the PFZ and the SAZ.

4.1. Seasonal and Spatial Contributors to the Intercruise $\delta^{15}N$ Differences

While all our foraminifer samples were collected from the Southern Ocean south of Africa, the winter and late-summer voyages are separated by 17–38° longitude, falling into different sectors (Atlantic and Indian, respectively). The complex frontal geometry (e.g., branching) and proximity of the Agulhas retroflection (Figure 1b) make for a more dynamic hydrographic setting in the late-summer (i.e., Indian sector) transect (Belkin & Gordon, 1996; Lutjeharms & Valentine, 1984). This raises the question: how much of the winter foraminifer $\delta^{15}N$ elevation (by 4.6 ± 0.8‰ for tissue and 4.0 ± 1.5‰ for shells; Tables S2b and S2e) relative to late summer can be explained by spatial differences? One possibility is that the higher $\delta^{15}N$ of foraminifera on the winter transect could be caused by a higher-$\delta^{15}N$ nitrate source feeding the PFZ/SAZ mixed layer in the Atlantic relative to the Indian sector. However, we observe no such difference in UCDW or SAMW properties between the two transects.

The meridional gradient in mixed-layer nitrate $\delta^{15}N$ on the Indian/late-summer transect appears weak compared to winter/Atlantic gradient (compare dark blue lines in Figures 4a and 4b). Late-summer nitrate $\delta^{15}N$ plateaus into the northern SAZ and decreases across the STF, despite the continued and steepening northward decline in nitrate concentration along the same transect (light green line in Figure 4b). One possible explanation is the lowering of Indian SAZ mixed-layer nitrate $\delta^{15}N$ by cross-frontal mixing with low-$\delta^{15}N$ Agulhas nitrate. Our own measurements of mixed-layer nitrate in the Agulhas Retroflection (station M10 at 41.0°S; Figure 1b) exhibit anomalously low $\delta^{15}N$ values for the low nitrate concentration, deviating from the equatorward rise in $\delta^{15}N$ expected for progressive nitrate assimilation (northernmost station in Figure 4b; orange profile in Figure 2). This low-$\delta^{15}N$ signature has been observed previously in Agulhas rings (Campbell, 2016; Smart, 2014; Smart et al., 2015) and in the Agulhas current itself (Sinyanya et al., 2020) and may derive from near-complete consumption of relatively low-$\delta^{15}N$ thermocline nitrate, possibly lowered by N_2-fixation (implied by excess nitrate relative to phosphate, that is, high N* concentrations; Gruber & Sarmiento, 1997), in the western subtropical Indian Ocean. A consequence of mixing with this low-$\delta^{15}N$, low-concentration Agulhas nitrate would be to weaken the $\delta^{15}N$ gradient (at least slightly) but strengthen the concentration gradient across the SAZ mixed layer, potentially masking part of the summertime assimilation signal in this region. While cross-frontal exchange with the subtropics (via eddy mixing; Speer et al., 2000; McNeil et al., 2001) has been estimated to contribute minimally to SAZ mixed-layer nitrate south of Australia, the contribution may be more significant in this dynamic region south of Africa. Regardless of any potential Agulhas influence, the SAZ and PFZ mixed layers of the late-summer/Indian transect host higher nitrate $\delta^{15}N$ than those of the winter/Atlantic transect, as would be expected from the increased ratio of nitrate consumption relative to supply in the summertime Southern Ocean.

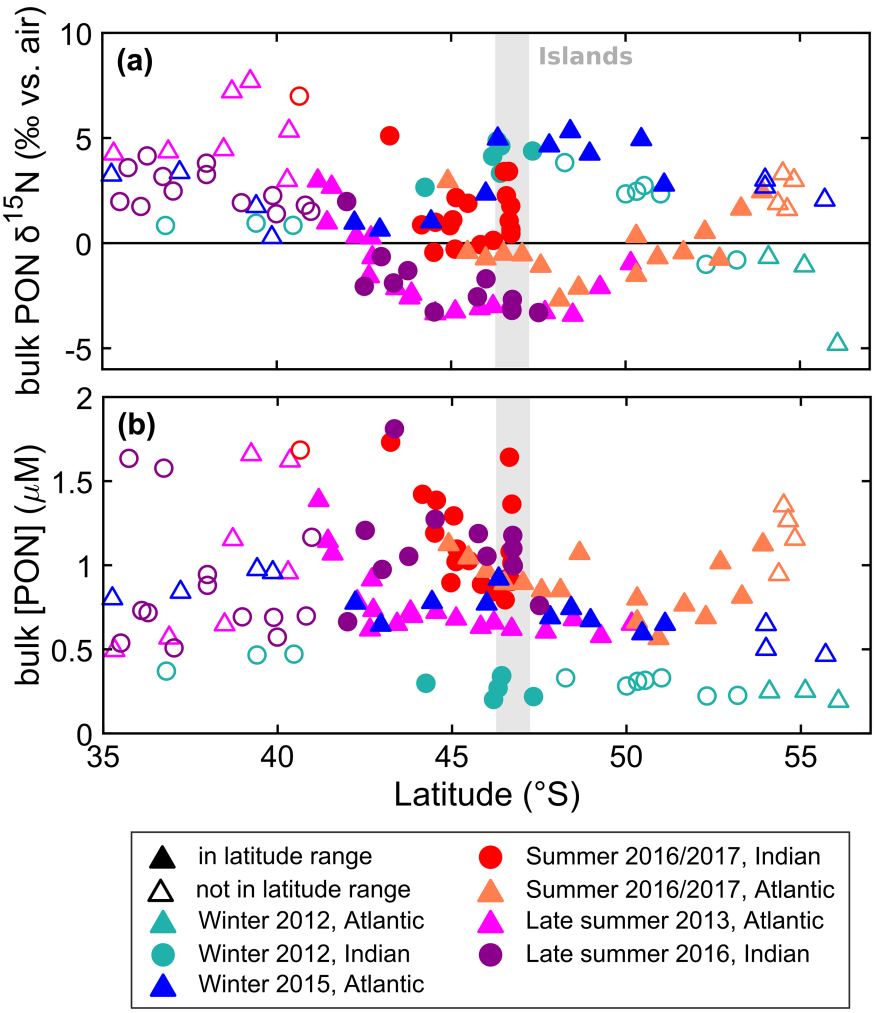

Figure 7. Compilation of bulk (>0.7 μm) suspended PON (a) $\delta^{15}N$ (‰ versus N_2 in air) and (b) concentration (μM) data from underway surface collections in the Southern Ocean south of Africa (0–42°E). Triangles denote measurements from the Atlantic Sector (west of 20°E) and circles denote those from the Indian Sector (east of 20°E). Blue symbols are used for winter, orange/red symbols for midsummer, and pink/purple for late summer. Symbols are filled if they fall within the same latitude range as our foraminifer tow collections from that sector. Circles within the vertical gray bar are excluded from our calculations, as these samples were collected nearshore and downstream of Marion Island, where we have no foraminifer data.

Hypothetically, higher foraminifer $\delta^{15}N$ in winter versus late summer could be explained by a higher $\delta^{15}N$ of foraminiferal food sources available in the Atlantic sector than in the Indian sector. Assuming that nitrate is the dominant control on the $\delta^{15}N$ of PON, such a difference in food $\delta^{15}N$ is unlikely in the absence of substantial longitudinal differences in the nitrate source or isotope effect of nitrate assimilation. However, different environmental conditions could favor different plankton assemblages and thus bulk PON properties. We test for Indian versus Atlantic differences (divided at 20°E) in the $\delta^{15}N$ of bulk suspended PON using data from our cruises plus additional bulk samples from the region (see section 2; Figure 7). We observe very little difference in the $\delta^{15}N$ of PON (Figure 7a) between the Atlantic and Indian sectors in winter (Atlantic: 3.2 ± 0.9‰ vs. Indian: 4.0 ± 0.3‰, $n = 4$ and 6, respectively), midsummer (Atlantic: 0.6 ± 1.2‰ vs. Indian: 0.8 ± 0.4‰, $n = 3$ and 7, respectively) or late summer (Atlantic: −2.1 ± 0.4‰ vs. Indian: −2.0 ± 0.4‰, $n = 13$ and 12, respectively); for this comparison, averages are calculated from the data points shown in Figure 7 that are within the latitudinal range of our net tows (indicated by filled symbols) and cover both the Indian and Atlantic sectors (i.e., where filled circles and triangles overlap in latitude). Even the broader latitudinal patterns in PON $\delta^{15}N$ are remarkably similar between sectors, excluding those collected nearshore

Table 2
Comparison Between Southern Ocean and Sargasso Sea Foraminifer $\delta^{15}N$ Relationships With Bulk PON and Nitrate Consumed

	Foraminifer minus bulk PON $\delta^{15}N$ difference (‰)						Foraminifer minus nitrate-consumed $\delta^{15}N$ difference (‰)					
	SAZ/PFZ[a]			Sargasso Sea[b]			SAZ/PFZ[c]			Sargasso Sea[d]		
Species	Mean	SE	*n*	Mean	SE	*n*	Mean	SE	*n*	Mean	SE	*n*
G. bulloides	**3.1**	0.3	9	**2.2**	0.2	3	**0.7**	0.6	10	**0.1**	0.1	4
G. inflata	**3.8**	0.4	9	**3.3**	0.8	3	**2.5**	0.8	11	**0.7**	0.4	5
G. truncatulinoides	**3.4**	0.3	10	**2.6**	0.7	5	**1.9**	0.9	12	**0.7**	0.2	8
O. universa	**1.2**	0.7	5	**2.0**	0.6	5	**-0.3**	1.2	7	**−0.2**	0.3	9
G. hirsuta	—	—	0	**3.1**	0.4	3	**4.5**	0.5	2	**1.1**	0.3	5
G. glutinata	**2.3**	0.7	6	**1.9**	0.6	2	**−0.6**	1.5	6	**−0.1**	0.3	3
N. incompta	**1.7**	1.5	2	—	—	0	**−1.2**	1.3	2	—	—	0
T. quinqueloba	**1.5**	1.6	4	—	—	0	**−0.5**	1.6	5	—	—	0
N. pachyderma	**2.9**	0.8	3	—	—	0	**1.4**	1.9	3	—	—	0
ALL tows	**3.2**	0.2	10	**2.5**	0.6	5	**1.7**	0.8	12	**0.2**	0.2	10

Note. Here we compare the $\delta^{15}N$ offset of foraminifer tissue from bulk (>0.7 μm) suspended PON (left-hand side) and from nitrate consumed (right-hand side) in two different nutrient regimes, the African PFZ/SAZ (where surface nitrate is partially consumed) and the Sargasso Sea (where surface nitrate is fully consumed). Mean (bold) and standard error (with n = number of tow sites) are given for each species and overall (bottom row).
[a]Here we use surface collections to approximate mixed-layer average suspended PON-$\delta^{15}N$. [b]Here we use euphotic-zone averaged bulk PON-$\delta^{15}N$. [c]In the case of incomplete nitrate consumption (PFZ/SAZ), we estimate (using a simple two end-member mixing model) the $\delta^{15}N$ of nitrate consumed during the productive summer season from the $\delta^{15}N$ and concentration at the start (calculated) and end (measured) of the growing season. The properties of mixed-layer nitrate at the start of spring are calculated using two end-member isotope models as described in section 4.3. We average the results (0.7‰ for the Rayleigh case, 1.4‰ for steady state) to get a $\delta^{15}N$ of 1.0‰ for nitrate consumed in the SAZ/PFZ. [d]In the case of complete nitrate consumption (Sargasso Sea), we take the $\delta^{15}N$ of the thermocline source (~2.5‰ for nitrate+nitrite) as the $\delta^{15}N$ of nitrate consumed annually in the euphotic zone.

and downstream of Marion Island (circles within the vertical gray bar), where we have no foraminifer data. The concentration of PON (Figure 7b) does differ between the Atlantic and Indian sectors in the winter (Atlantic: 0.8 ± 0.0 μM vs. Indian: 0.3 ± 0.0 μM, n = 4 and 6, respectively) and late summer (Atlantic: 0.7 ± 0.0 μM vs. Indian: 1.1 ± 0.1 μM, n = 13 and 12, respectively) but not in midsummer (Atlantic: 1.0 ± 0.0 μM vs. Indian: 1.0 ± 0.1 μM, n = 3 and 7, respectively).

Another possibility is that the observed winter versus summer differences in foraminifer $\delta^{15}N$ are the result of seasonal changes in foraminifer species assemblage and size distribution. In order to avoid overinterpretation of data with large gaps, we focus our discussion on the three most abundant and commonly occurring species in our collections: *G. inflata*, *G. truncatulinoides*, and *G. bulloides*. For example, the lower average $\delta^{15}N$ of foraminifer tissue and shells in late summer could be due to the abundance of *G. bulloides* in the late-summer tow collections, which typically have a lower $\delta^{15}N$ than *G. inflata* and *G. truncatulinoides* in the same tow (by 1.0‰ and 0.4‰ on average, respectively). Similarly, *G. bulloides* dominates the more polar tows on the late-summer transect (Figure 2), which could steepen the meridional gradient in foraminifer $\delta^{15}N$. While such effects may contribute to the overall average seasonal differences (black trendline in Figure 6e), we also observe these patterns within the same species (color trendlines in Figure 6e). In summary, differences in regional nitrate sources, PON properties and foraminifer assemblages appear to contribute little to the observed Atlantic/winter versus Indian/late-summer differences in N isotope properties of the PFZ and SAZ mixed layers. We thus conclude that the differences between cruises primarily reflect seasonal changes in the PFZ/SAZ and refer to them as such below.

4.2. Control of Foraminifer $\delta^{15}N$ by PON $\delta^{15}N$

The seasonally inconsistent effect of seawater nitrate $\delta^{15}N$ on foraminifer $\delta^{15}N$ (Figures 6b and 6f), in terms of direction (positive in winter, negative in late summer) and absolute offset (small in winter, large in late summer), leads us to consider the immediate N sources available to foraminifera and their causal role in determining foraminifer $\delta^{15}N$. The most consistent relationship we observe, regardless of season, is between foraminifer $\delta^{15}N$ and bulk suspended PON $\delta^{15}N$ (Figures 6c and 6g). In both winter and late summer, the

bulk PON-foraminifer relationship is near 1:1 and the offset is around 3‰, the typical $\delta^{15}N$ difference between heterotrophs and their diet (Checkley & Miller, 1989; Minagawa & Wada, 1984). This $\delta^{15}N$ difference between foraminifer tissue and bulk suspended PON (across all species; 3.2 ± 0.2‰, $n = 10$) is similar to that observed in the subtropical North Atlantic (2.5 ± 0.6‰; $n = 5$; Table 2). The bulk suspended PON with which we compare our foraminifera contains all particles larger than the pore size of the filter and, therefore, includes phytoplankton (from the larger diatoms and coccolithophores through to small cyanobacteria like *Synechoccocus*), detritus and the occasional zooplankton, but excludes bacteria smaller than 0.7 μm unless they are particle-associated. In terms of biomass, large phytoplankton likely contribute the most to both living and detrital organic matter in the Southern Ocean mixed layer (Buitenhuis et al., 2013, and references therein). While there is also a strong correlation between PFZ/SAZ foraminifera (dominated by nondinoflagellate-bearing species) and the larger size fractions of PON (caught by the same net tow; Figures 6d and 6h), the small $\delta^{15}N$ offset (0.2 ± 0.3‰; $n = 12$) between the two groups suggests that the relationship is driven largely by a common food source rather than by foraminifera feeding heavily on zooplankton and/or their detritus. We return to this at the end of section 4.2. The consistent positive effect of bulk suspended PON on foraminifer $\delta^{15}N$ suggests that the $\delta^{15}N$ of foraminifera more closely resembles that of their diet rather than the $\delta^{15}N$ of ambient seawater nitrate, which is consistent with foraminifera acquiring N mostly from their particulate food (Bé et al., 1977; Spindler et al., 1984; Uhle et al., 1997), rather than from nitrate+nitrite directly, despite high concentrations of ambient nitrate in the mixed layer. This interpretation relies on two assumptions: (1) The $\delta^{15}N$ of bulk suspended PON in surface waters approximates the $\delta^{15}N$ of bulk suspended PON at the depth of the tow collection, and (2) bulk suspended PON is a reasonable measure of the PON consumed by foraminifera.

First, the $\delta^{15}N$ of suspended PON has been found to increase with depth in the open ocean, particularly through the upper 500 m of the water column (by ~6–10‰), due to the preferential removal of ^{14}N from particles during heterotrophic degradation (Altabet et al., 1991; Altabet & McCarthy, 1986; Hannides et al., 2013; Saino & Hattori, 1980). This $\delta^{15}N$ increase is typically accompanied by a decrease in the concentration and an increase in the C:N ratio of suspended PON with depth, signaling the more rapid decomposition of labile, N-rich components like proteins (Altabet & McCarthy, 1986; Lehmann et al., 2002). However, all of our tow collections were made within the upper 100 m of the water column, usually within a uniformly high-chlorophyll mixed layer (although local subsurface maxima were targeted when present, i.e., at M2, M9, and W1), suggesting a relatively even distribution of phytoplankton particles through the mixed layer at most stations. Depth-profiles of suspended PON $\delta^{15}N$ from the PFZ/SAZ south of Africa exhibit an overall increase in $\delta^{15}N$ from near the surface to 100 m of ~1‰ in midsummer (2016/2017 profiles between 0°E and 40°E; warm colors in Figure S3) and of <0.5‰ in winter (2017 profiles along 30°E; cool colors in Figure S3). In addition, existing late-summer measurements from the Indian sector indicate minimal increases of ≤0.5‰ in PON-$\delta^{15}N$ with depth in the upper 100 m of the water column (high-nutrient, low-chlorophyll off-plateau sites near Kerguelen; Trull et al., 2008). Furthermore, the average C:N ratios of suspended PON increase by less than 0.5 over the same interval in these profiles (Trull et al., 2008) and show no consistent depth trend in the Atlantic sector (Martiny et al., 2014). Therefore, we consider our underway collections of suspended PON to be a reasonable approximation for the $\delta^{15}N$ of suspended PON at the tow depth, at least during winter and late summer when foraminifera were collected.

Second, some foraminifer species feed preferentially on specific types of PON, which may differ in $\delta^{15}N$ from bulk suspended PON. In high-nutrient waters like the Southern Ocean, *G. bulloides* appears to follow the chlorophyll maximum (Mortyn & Charles, 2003) while *G. inflata* and *G. truncatulinoides* are thought to rely mostly on detrital particles due to their deeper average depth habitat (with peak abundances observed at 50–300 m and 100–600 m, respectively, in the summertime Atlantic sector; Mortyn & Charles, 2003). Clearly, *G. inflata* and *G. truncatulinoides* do spend some portion of their life cycle within the mixed layer (evident from their abundance in our net tows), but these periods may coincide with reproduction and be relatively short-lived, at least for *G. truncatulinoides*, which appears to only reproduce annually (Schiebel et al., 2002; Schiebel & Hemleben, 2017; Weyl, 1978). The partial dependence on more degraded PON with a higher $\delta^{15}N$ is one explanation for the higher $\delta^{15}N$ of *G. inflata*, *G. truncatulinoides*, and *G. hirsuta* relative to shallow-dwellers like *O. universa* in subtropical environments (the other being the absence of dinoflagellate symbionts, which we discuss below; Ren et al., 2012).

In contrast, *O. universa* is thought to be mostly carnivorous, preying on other zooplankton like copepods (Bé et al., 1977; Spindler et al., 1984), and would, therefore, be expected to have a higher-$\delta^{15}N$ diet than that of herbivorous foraminifera. At the same time, this species has dinoflagellate endosymbionts, which act to weaken their host's trophic $\delta^{15}N$ elevation by taking up low-$\delta^{15}N$ ammonium that would otherwise be excreted by the foraminifer (Ren et al., 2012; Uhle et al., 1999). It has been proposed that this internal N recycling (and thus lack of ammonium efflux) explains the lower $\delta^{15}N$ of *O. universa* relative to symbiont-barren species, at least in the (sub)tropical ocean (Ren et al., 2012; Smart et al., 2018). In the SAZ/PFZ, *O. universa* are, on average, 1.3 ± 0.5‰ ($n = 7$) lower in $\delta^{15}N$ (i.e., approximately half a trophic level lower) than nondinoflagellate bearers from the same tow. While the scarcity of *O. universa* in our tow collections prevents us from drawing more robust conclusions about this species in the Southern Ocean, their symbionts might contribute either directly (as a major constituent of the cytoplasm we measure as foraminifer "tissue"; Spero, 1987) or indirectly (via biochemical exchanges) to the lower measured $\delta^{15}N$ of *O. universa* relative to other species. Given the lower temperature bound of ~10 °C for *O. universa* (Bé, 1977; Darling & Wade, 2008), it is also possible that these individuals were transported into subpolar waters by warm-core eddies or by mixing across the STF and that local conditions are not representative of their primary habitat. A similar mechanism was proposed to explain the abundance of *O. universa* (up to 7%) in sediment traps during winter in the central SAZ (47°S) south of Tasmania (King & Howard, 2003).

The $\delta^{15}N$ elevation that we observe for *G. bulloides* relative to surface-suspended PON (at the same station) remains fairly constant from winter (2.9 ± 0.9‰; $n = 2$) to late summer (3.2 ± 0.3‰; $n = 7$), suggesting a close coupling between this species and phytoplankton in the surface ocean. On average, the $\delta^{15}N$ of *G. bulloides* is lower than that of *G. inflata* and *G. truncatulinoides* (by 1.0 ± 0.3‰ [$n = 9$] and 0.4 ± 0.3‰ [$n = 10$], respectively) from the same tows. Given that none of these species have dinoflagellate endosymbionts, the differences might imply a higher-$\delta^{15}N$ diet for the latter two species (i.e., feeding on more degraded PON below 100 m depth and/or on zooplankton-derived PON). Our measured offsets are in line with observations from the Sargasso Sea, where the tissue $\delta^{15}N$ of tow-caught *G. bulloides* is ~0.6‰ lower than the annual averages for *G. inflata* and *G. truncatulinoides* (Smart et al., 2018). While our *G. inflata*-*G. bulloides* offset is similar between seasons (1.4 ± 0.2‰ in winter and 0.8 ± 0.4‰ in late summer), the *G. truncatulinoides*-*G. bulloides* offset varies from 1.3 ± 0.2‰ in winter to 0.0 ± 0.3‰ in late summer. The late-summer convergence of *G. truncatulinoides* $\delta^{15}N$ on *G. bulloides* $\delta^{15}N$ may reflect a dietary shift in *G. truncatulinoides* from more degraded/zooplankton-derived PON in winter to a phytoplankton-based diet in summer, perhaps due to its seasonal/annual migration into shallow waters (e.g., for reproduction). This is supported by consistently higher $\delta^{15}N$ values (by 1.2‰ on average; $n = 9$) for *G. truncatulinoides* shells (recording long-term conditions at their primary habitat) compared to tissue (capturing recent activity such as feeding at the tow collection depth) from the same net tows.

In summary, the $\delta^{15}N$ of foraminifera appears to be more closely tied to the $\delta^{15}N$ of PON forms than to that of dissolved nitrate. On the whole, the observed $\delta^{15}N$ relationships (among different foraminifer species, as well as between foraminifera, other zooplankton and bulk suspended PON) point to a similar, largely phytoplankton-(and detritus-)based diet for nondinoflagellate-bearing foraminifera living in the SAZ/PFZ.

4.3. Seasonality in Bulk PON

If PON is indeed the main control on foraminifer $\delta^{15}N$, then processes affecting spatial patterns and seasonality in PON $\delta^{15}N$ warrant our attention. The first process we consider is nitrate assimilation. Nitrate is drawn down rapidly (although not to completion) during the productive season, fueling the phytoplankton blooms that characterize spring and summer in the Southern Ocean. Depending on the rate of nitrate resupply to the summertime mixed layer, the N isotope dynamics of the remaining nitrate and the PON produced can be approximated by a simple Rayleigh model (assuming no nitrate resupply) or steady-state model (assuming continuous resupply). While the PFZ and SAZ exhibit aspects of both closed- (e.g., stratification and nitrate depletion) and open- (e.g., equatorward transport) system behavior during the summer (Altabet & François, 2001; DiFiore et al., 2006), we can use these two endmember models to calculate the range of PON $\delta^{15}N$ values expected for the region south of Africa.

For each zone, we estimate the fraction of nitrate remaining at the end of summer using the average concentration difference between the surface and 150 m depth; ~0.88 for the PFZ, ~0.78 for the SAZ (Lourey et al., 2003). We then back-calculate the $\delta^{15}N$ of "initial" mixed-layer nitrate (i.e., at the start of spring) for each model, using literature values for the isotope effect of nitrate assimilation; $\varepsilon \sim 4.9–6.1‰$ in the PFZ (Fripiat et al., 2019) and $\varepsilon \sim 7–9‰$ in the SAZ (DiFiore et al., 2006; Lourey et al., 2003). Using the same parameters, we estimate the $\delta^{15}N$ of PON being produced by the end of the summer season (i.e., the instantaneous product) to be +1.2 to +2.4‰ or +1.2 to +2.4‰ in the PFZ, and −0.4 to +1.7‰ or −0.1 to +1.9‰ in the SAZ (for steady state or Rayleigh models, respectively). If all the PON produced during the growing season accumulated in the mixed layer, it would have a $\delta^{15}N$ of +0.8 to +2.1‰ in the PFZ and −1.3 to +1.0‰ in the SAZ. These values are substantially higher than what we observe in late-summer surface waters, particularly for the PFZ (where PON $\delta^{15}N$ averages $-2.8 \pm 0.3‰$; $n = 5$). Conversely, the calculated $\delta^{15}N$ values are well below our bulk suspended PON measurements for the winter PFZ (averaging $+3.9 \pm 0.6‰$; $n = 7$). Lourey et al. (2003) describe similar results from the Pacific sector south of Australia: the $\delta^{15}N$ of bulk suspended PON in the late-summer PFZ (and possibly SAZ) is too low to be explained by nitrate depletion alone, which the authors concluded is most likely due to ammonium recycling in the late-summer mixed layer. This explanation is also consistent with our results.

Ammonium originates from two main sources: bacterial decomposition of PON (Lehmann et al., 2002) and excretion by zooplankton (Checkley & Miller, 1989). Isotopic fractionation during these processes (specifically, deamination) causes ammonium to have a low $\delta^{15}N$ relative to nitrate. Its subsequent assimilation by phytoplankton can, therefore, lower the $\delta^{15}N$ of the mixed-layer PON pool. Ultimately, the retention of ^{14}N within the mixed layer must be linked to the preferential export of ^{15}N-rich particles (like larger, faster-sinking phytoplankton or zooplankton fecal pellets; Altabet & Small, 1990; Möbius, 2013). The use of ammonium as an alternative N source by phytoplankton has been observed previously in the Southern Ocean (Elskens et al., 2002; Glibert et al., 1982; Koike et al., 1986; Sambrotto & Mace, 2000), including across PFZ and SAZ surface waters of the African sector (Joubert et al., 2011; Thomalla et al., 2011). In fact, the meridional gradient in suspended PON $\delta^{15}N$ (and we propose, by extension, in the $\delta^{15}N$ of foraminifera) across the late-summer Pacific PFZ/SAZ was hypothesized to be at least partly driven by more intense ammonium recycling lowering PON $\delta^{15}N$ in the PFZ relative to the SAZ (Lourey et al., 2003), rather than being solely a consequence of the south-to-north increase in nitrate consumption that causes the northward rise in nitrate $\delta^{15}N$ (Sigman, Altabet, McCorkle, et al., 1999).

As for the wintertime, when light conditions deteriorate (due to deeper mixing and turbulence, as well as less insolation), the rate ratio of nitrate assimilation to nitrate resupply is lower, and thus nitrate and any PON produced from it would be expected to have a lower $\delta^{15}N$ than during peak (midsummer) nitrate drawdown. Yet the winter PFZ mixed layer hosts the highest-$\delta^{15}N$ PON, even compared to midsummer measurements from the same transects (compare blue vs. orange triangles and turquoise vs. red circles in Figure 7a). As with the anomalously low $\delta^{15}N$ of late-summer PON, higher-than-predicted "early season" (i.e., prebloom) PON $\delta^{15}N$ has been noted previously in the Southern Ocean (Altabet & François, 1994; Altabet & François, 2001; Lourey et al., 2003) and in the subarctic Pacific (Wu et al., 1997). A likely explanation for this phenomenon is the remineralization of PON remaining in the mixed layer during the long, less productive winter season. As described previously, bacterially mediated decomposition of suspended PON leaves remaining particles elevated in $\delta^{15}N$ (Altabet et al., 1991; Altabet & McCarthy, 1986; Saino & Hattori, 1980) and could, therefore, drive at least part of the ~8‰ summer-to-winter increase in PON $\delta^{15}N$ observed in the PFZ. While remineralization within the mixed layer likely occurs year-round, the ammonium released from decomposition during summer would be reassimilated into new biomass (i.e., PON), along with continued production of PON from nitrate, causing decomposition to have a weaker effect on PON $\delta^{15}N$ outside of the winter season. In addition, during the winter, the heterotrophic activity and packaging processes that remove partially decomposed organic matter from the surface may be at a minimum. Another contributor to the PON $\delta^{15}N$ rise might be a return to nitrate assimilation, but this switch alone could not explain more than ~3‰ of the observed ~8‰ increase, and nitrate assimilation is an energetically expensive process (Dorch, 1990) that seems less likely under winter conditions (Philibert et al., 2015). In summary, while nitrate assimilation appears to be the overarching driver of bulk PON $\delta^{15}N$ in Southern Ocean surface waters during the productive spring and summer seasons, internal

mixed-layer N cycling processes seem to be important additional controls on PON (and indirectly, foraminifer) $\delta^{15}N$ during the rest of the year.

4.4. Implications for the Foraminifer-Bound $\delta^{15}N$ Paleo-Proxy

This study confirms that, for the nitrate-rich environment of the Southern Ocean, feeding causes living planktic foraminifera (tissue and shell) to track the $\delta^{15}N$ of upper-ocean PON rather than that of nitrate directly. Furthermore, the $\delta^{15}N$ of bulk PON in modern SAZ/PFZ surface waters, and therefore the $\delta^{15}N$ of the foraminifera that feed upon it, does not simply reflect nitrate assimilation but also records (1) ammonium recycling in late summer and (2) microbial decomposition in winter. Here, we explore how these "nonnitrate-assimilation" processes might be reflected in the $\delta^{15}N$ of foraminifer shells accumulating in seafloor sediments.

The ability to reconstruct the degree of surface nitrate consumption from the $\delta^{15}N$ of exported PON relies on the mass balance condition: that all the N consumed by phytoplankton within the mixed layer is (eventually) exported as PON and does not accumulate indefinitely in the surface ocean or undergo substantial lateral export (as PON, ammonium, etc.; Altabet & François, 1994; their Figure 9). The seasonal partitioning of ^{14}N and ^{15}N between different mixed-layer N pools does not violate this condition of mass balance, as long as it is applied on annual or longer time scales. A greater concern for sinking PON as a proxy for nitrate consumption is isotopic alteration of the organic matter in the water column or surface sediments, which raises its $\delta^{15}N$ by 0–5‰ (Altabet & François, 1994; François et al., 1992; Thunell et al., 2004). The potential for climate-modulated, temporal variation in the degree of isotopic alteration makes this "diagenetic offset" (Altabet & François, 1994) particularly difficult to correct for (e.g., Martínez-García et al., 2014).

On the one hand, foraminifer shell-bound (not cytoplasm) organic matter is physically protected from bacterially mediated decay by the mineral matrix, thus mitigating the concern of diagenesis as shells sink through the water column and are incorporated into the sediments. Indeed, changes in shell-bound $\delta^{15}N$ from net tows to seafloor sediments are comparatively small (Ren et al., 2012), with an average increase of ~0.6‰ (Smart et al., 2018). On the other hand, foraminifera make up just one component of the total PON produced in and exported from the upper ocean and thus need not track the $\delta^{15}N$ of nitrate consumed annually (i.e., foraminifera are not constrained by the mass balance that applies to bulk sinking PON). Different species also peak in abundance at different times of year and may have different feeding preferences, depth habitats, and lifespans, further complicating the picture.

In order to assess the influence of upper ocean N cycling on SAZ/PFZ foraminifera-bound $\delta^{15}N$ recorded in sediments, we combine our isotopic data with information on the relative contributions of late-summer and winter to annual foraminifer production. Our net tows provide only a snapshot of mixed-layer foraminifer abundances and are limited to two seasons. Furthermore, the presence of a species within the upper ocean does not require that its production and export are significant during the season of observation; indeed, the greatest fluxes of planktic foraminifera are observed during episodic mass flux events (Schiebel, 2002). We therefore look to sediment trap data for the seasonality of the Southern Ocean foraminiferal flux. Sediment trap fluxes are not available for our region south of Africa, so we turn to the Australian SAZ/PFZ, which we expect to exhibit similar seasonal and spatial patterns in foraminifer production to the African SAZ/PFZ. Total mass flux and foraminiferal flux in the western Pacific sector are generally lower in the SAZ and higher in the PFZ, with local maxima at the SAF (highest overall) and STF boundaries (Honjo et al., 2000; King & Howard, 2001; King & Howard, 2003; Trull et al., 2001). Most traps in this region record a double peak in production, one in spring/midsummer and one in mid/late summer. In calculating the contribution of each season to the annual sinking flux, we take winter to be represented by the 3-month period, either June-July-August or July-August-September, depending on the site.

In the northern SAZ (45°S) east of New Zealand (just south of the STF), mass fluxes captured in a 1,000 m trap (Nodder & Northcote, 2001) were dominated by spring fluxes (68% in September-October-November), with lower fluxes in midsummer (13% in December-January-February), late summer (5% in March-April-May), and winter (14% in July-August-September). Foraminiferal fluxes in the same collections appear largely consistent with the mass fluxes (King & Howard, 2001), but with a slight (~2 week) lag, contributing to lower foraminiferal fluxes for winter (~7%) and higher for late summer (~16%). In a collection from the central SAZ (47°S) south of Tasmania (King & Howard, 2003), spring (October-November-December)

contributed 15–22%, midsummer (January-February-March) contributed 34–37%, late summer (April-May-June) contributed 39–42%, and winter (July-August-September) contributed 6% to the annual total of foraminifera reaching 3,800 m depth. At the SAF (51°S; 3,100 m depth) and PFZ (54°S; 1,500 m depth) sites south of Tasmania, the winter period was not captured, but low foraminiferal fluxes recorded in September (King & Howard, 2003) suggest an annual contribution of <6%. Total mass fluxes and inorganic carbon fluxes from a PFZ (57°S) sediment trap south of New Zealand (Honjo et al., 2000) suggest smaller contributions to the annual mass flux from late summer (9% and 13%, respectively; March-April-May) and winter (~1% for both; June-July-August) compared to the SAZ, with spring (27% and 33%, respectively; September-October-November) and midsummer (63% and 53%, respectively; December-January-February) dominating the sinking flux at 1,000 m. Based on these data, the seasons in which internal mixed-layer N cycling dominates (late summer and winter) are the seasons that contribute the least to the annual total foraminifera sinking to the sediments in the PFZ. In the SAZ, winter production may contribute proportionally more shells to the sediments, but the effects of winter decomposition (on PON and foraminifer $\delta^{15}N$) appear to be weaker here than in the PFZ mixed layer. Ammonium recycling, on the other hand, appears to be important, at least in the southern/central SAZ, and late-summer foraminifer fluxes can be substantial.

To test the influence of these "peripheral" seasons on the $\delta^{15}N$ of the modern annual foraminifer flux, we calculate the expected $\delta^{15}N$ of a sediment sample from the PFZ where 86% of the foraminifera derive from spring plus midsummer, 13% derive from late summer, and 1% derive from winter (based on the inorganic carbon fluxes of Honjo et al., 2000). We repeat this exercise for the SAZ, assuming 52% of shells derive from spring plus midsummer, 42% are from late summer, and 6% are from winter (using the foraminiferal fluxes of King & Howard, 2003). In both cases, we use the overall SAZ/PFZ average foraminifer tissue $\delta^{15}N$ ("naturally weighted" toward the $\delta^{15}N$ of more abundant species; combining all the tissue $\delta^{15}N$ data from Table 1) as an approximation for the shell flux $\delta^{15}N$ in winter (5.4‰) and late summer (1.0‰), and we estimate the spring+midsummer foraminifer $\delta^{15}N$ as the average spring+midsummer PON $\delta^{15}N$ (orange and red symbols in Figure 7a) plus our average observed trophic elevation (Table 2; i.e., 0.7 + 3.2 = 3.9‰). Presumably, the $\delta^{15}N$ of the foraminiferal flux corresponds to surface mixed-layer conditions up to a month earlier, but we do not attempt to correct for this here.

From this calculation, we can develop a first sense of the degree to which winter and late-summer fluxes "skew" the sediment record away from the spring+midsummer nitrate consumption signal that we hope to reconstruct using foraminifer-bound $\delta^{15}N$. For the PFZ, the resulting sediment mixture has a $\delta^{15}N$ that is 0.4‰ lower than the $\delta^{15}N$ of the spring+midsummer shells alone. For the SAZ, the resulting mixture is 1.1‰ lower than the spring+midsummer $\delta^{15}N$. Perhaps a more realistic test is to use PFZ- and SAZ-specific ranges for the $\delta^{15}N$ of the foraminiferal flux in each season; 6.0‰ to 8.2‰ and 3.0‰ to 6.0‰ in winter, −0.8‰ to 1.8‰ and −0.6‰ to 3.6‰ in late summer, and 2.3‰ to 3.5‰ and 2.4‰ to 7.2‰ in spring+midsummer for the PFZ and SAZ, respectively. Using the same seasonal contributions as before, PFZ sediments are 0.2–0.4‰ lower and SAZ sediments are 1.2–1.6‰ lower than they would be if made up of spring+midsummer shells only (compare rows (a) with rows (b) in Table 3; or the color difference between "Modern" and the top corners of the triangles in Figure 8).

The results confirm that, under today's conditions, the effect of nonnitrate-assimilation processes (i.e., mixed-layer N cycling) is greater in the SAZ (Figure 8b) than in the PFZ (Figure 8a). The lowered $\delta^{15}N$ for both PFZ and SAZ sediments suggest that, on balance, late-summer ammonium recycling (which acts to lower shell-assemblage $\delta^{15}N$; compare rows (a) with rows (d) in Table 3) has a stronger influence on the sediments than does winter decomposition (which acts to raise shell-assemblage $\delta^{15}N$; compare rows (a) with rows (c) in Table 3). In general, under modern conditions, the two processes oppose each other in their $\delta^{15}N$ effects, and the winter shell flux is minor. In summary, these preliminary calculations suggest that seasonality influences the annually averaged value of foraminifer-bound $\delta^{15}N$ so as to underpredict the degree of nitrate consumption. However, such a seasonality-induced bias only affects paleoceanographic reconstructions of changes in the degree of nitrate consumption if this seasonality has changed over time.

Accordingly, we consider briefly how changes in the seasonality of the Southern Ocean N cycle over the glacial-interglacial transition could affect the foraminifer-bound $\delta^{15}N$ change observed in the sediment record. In the AZ, a reduced supply of nutrients to surface waters during glacial periods (François et al., 1997; Kemeny et al., 2018) could lead to an earlier switch to ammonium-based phytoplankton production

Table 3
Effects of Varying Seasonal Contributions on the Annual Total Foraminifer Flux $\delta^{15}N$ in the PFZ and SAZ

		Spring + summer		Late summer		Winter		Annual total	
Zone	Scenario	Foram. $\delta^{15}N$ (‰)	Contrib. (%)	Foram. $\delta^{15}N$ (‰)	Contrib. (%)	Foram. $\delta^{15}N$ (‰)	Contrib. (%)	Foram. $\delta^{15}N$ (‰)	Contrib. (%)
PFZ	(a) Modern[a]	2.3–3.5	86	−0.8–1.8	13	6.0–8.2	1	**1.9–3.3**	100
	(b) Only spring+summer	2.3–3.5	100	—	0	—	0	**2.3–3.5**	100
	(c) No winter	2.3–3.5	87	−0.8–1.8	13	—	0	**1.9–3.3**	100
	(d) No late-summer	2.3–3.5	99	—	0	6.0–8.2	1	**2.3–3.6**	100
	(e) No spring+summer	—	0	−0.8–1.8	93	6.0–8.2	7	**−0.3–2.3**	100
SAZ	(a) Modern[b]	2.4–7.2	52	−0.6–3.6	42	3.0–6.0	6	**1.2–5.6**	100
	(b) Only spring+summer	2.4–7.2	100	—	0	—	0	**2.4–7.2**	100
	(c) No winter	2.4–7.2	55	−0.6-3.6	45	—	0	**1.1–5.6**	100
	(d) No late-summer	2.4–7.2	90	—	0	3.0–6.0	10	**2.5–7.1**	100
	(e) No spring+summer	—	0	−0.6–3.6	88	3.0–6.0	13	**−0.2–3.9**	100

Note. For the foraminifer flux $\delta^{15}N$ ranges in each season, we use our measurements of tissue $\delta^{15}N$ where available (winter and late summer) and estimate the spring+summer range from PON $\delta^{15}N$ and the average trophic elevation as described in section 4.4. Annual total $\delta^{15}N$ ranges are shown in bold, and underlined in the case of modern conditions. The average results of the ranges presented in this table are illustrated by Figure 8.
[a]Modern PFZ seasonal flux contributions calculated from Honjo et al. (2000). [b]Modern SAZ seasonal flux contributions calculated from King and Howard (2003).

in the Southern Ocean than occurs today (Studer et al., 2015). It is possible that this would then increase the contribution of "late-summer-like" foraminifera (with a low $\delta^{15}N$) to the total shell assemblage in PFZ sediments during ice ages (approximate direction indicated by the arrow in Figure 8a). Indeed, under today's conditions, our data imply a larger $\delta^{15}N$ offset between foraminifera and nitrate consumed in subpolar surface waters (1.7 ± 0.8; $n = 12$) than in the Sargasso Sea (0.2 ± 0.2; $n = 10$; right-hand columns in Table 2). This appears to stem largely from a lower $\delta^{15}N$ for bulk PON relative to nitrate consumed in the Sargasso Sea, consistent with a greater dependence on ammonium by autotrophs in this subtropical ecosystem. Under the much lower nitrate supply rates calculated for the glacial AZ (Kemeny et al., 2018; Studer et al., 2015), Antarctic PON may adopt $\delta^{15}N$ relationships more similar to the modern Sargasso Sea; that is, becoming lower relative to the $\delta^{15}N$ of nitrate consumed in surface waters (Table 2). The effect on a

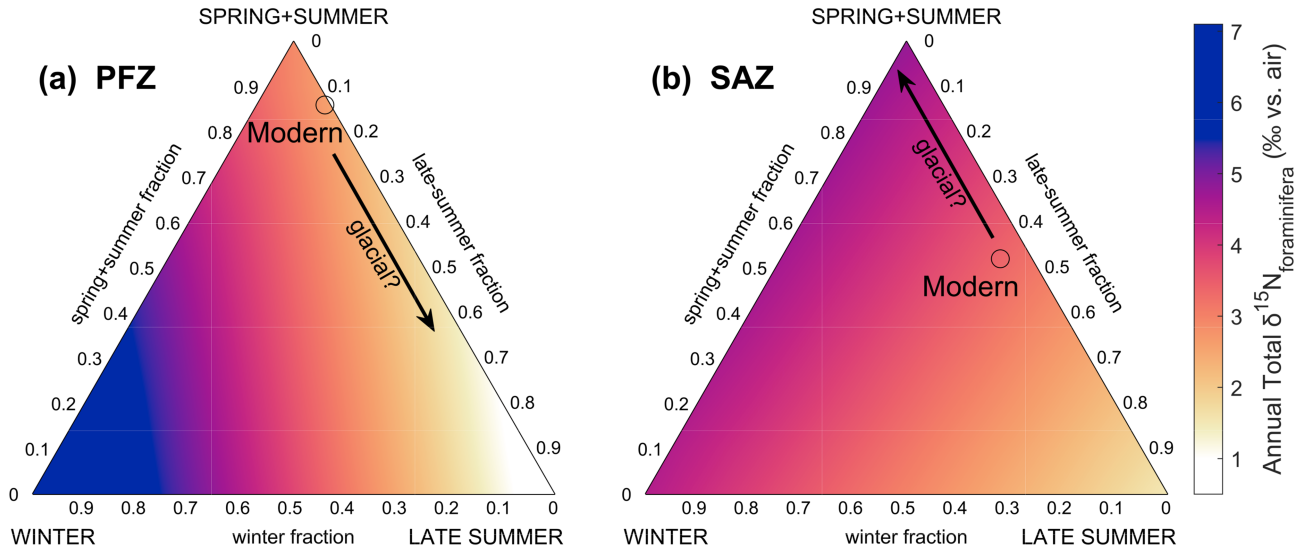

Figure 8. Ternary diagrams illustrating the effects of varying seasonal contributions (and their associated $\delta^{15}N$ values) to the $\delta^{15}N$ of annually accumulated foraminifera in (a) PFZ and (b) SAZ sediments. The black circle indicates the modern situation (based on seasonal flux data from sediment traps in the western Pacific SAZ/PFZ), and the black arrow indicates the approximate direction of change we might expect during glacial periods. This figure was created using the MATLAB routine "ternplot" (Sandrock and Afshari (2016)) and the colormap of Kovesi (2015).

foraminifer-bound $\delta^{15}N$ record from the PFZ would be to damp the glacial-interglacial signal, leading to underestimation of the ice age enhancement of nitrate drawdown in polar waters.

In contrast, enhanced iron-bearing-dust deposition to the glacial SAZ may prolong nitrate-based production at these latitudes (Martin, 1990; Martínez-García et al., 2014), increasing the proportion of "spring/midsummer-like" shells that more strongly follow nitrate consumption (approximate direction indicated by the arrow in Figure 8b). The effect on a foraminifer-bound $\delta^{15}N$ record from the SAZ would thus be to amplify the glacial-interglacial signal, leading to overestimation of the ice age enhancement of nitrate drawdown in subpolar waters. For example, in the case of the *G. bulloides* $\delta^{15}N$ record from the Atlantic SAZ (site ODP1090; Martínez-García et al., 2014), part of the 3–4‰ rise in glacial age shells could be explained by a reduction in ammonium-supported production compared to today. To place an upper bound on this effect, we consider the end-member case of zero ammonium recycling in the ice age SAZ. We estimate the $\delta^{15}N$ of modern *G. bulloides* shells in spring+midsummer from the bulk PON $\delta^{15}N$ in the northern SAZ (red symbols in Figure 7a) plus our average observed trophic elevation for *G. bulloides* (Table 2; i.e., ~5 + 3.1 ≈ 8.1‰). The result is ~1.4‰ higher than the measured $\delta^{15}N$ of *G. bulloides* in surface sediments at ODP1090 (6.7‰), which integrates over all seasons. Therefore, "correcting" this paleo-record for the ammonium recycling effect (which lowers the measured $\delta^{15}N$ of *G. bulloides* during interglacials but, in this end-member case, not during ice ages) would reduce the observed amplitude of the 3–4‰ glacial-interglacial signal by ~1–2‰ at most. This would leave the remaining (2–3‰) ice age elevation in foraminifer-bound $\delta^{15}N$ to be explained by enhanced nitrate drawdown.

While climate-driven change in N cycling seasonality may appear to present a concern, there would seem to be limits to its impact on foraminifer-bound $\delta^{15}N$ records. The PON, ammonium, and dissolved organic N in Southern Ocean surface waters ultimately derives from the assimilation of nitrate. Thus, the availability of both ammonium for late-summer assimilation and of PON for wintertime degradation are tied to nitrate assimilation-sourced biological production in the preceding spring and summer seasons. Given this, the annually integrated proportions of foraminifera recording the low-$\delta^{15}N$ late-summer signal or high-$\delta^{15}N$ winter signal, relative to the quantity of foraminifera recording the spring+summer PON signal of nitrate consumption, may well be highly conserved over time. Furthermore, much of the low-$\delta^{15}N$ ammonium released during wintertime PON degradation (Lehmann et al., 2002) will ultimately be reassimilated by phytoplankton in the following spring/summer, either directly as ammonium (Elskens et al., 2002; Glibert et al., 1982) or after nitrification to nitrate within the winter mixed layer (Smart et al., 2015), and likely help to balance the high-$\delta^{15}N$ of winter PON on an annual basis. These considerations argue against major changes in foraminifer-bound $\delta^{15}N$ over time that are independent of changes in the degree of nitrate consumption. Nevertheless, this remains to be tested, and foraminifer-bound $\delta^{15}N$ paleo-records from the Southern Ocean would clearly benefit from an improved understanding of upper-ocean particle dynamics in polar and subpolar waters.

To better constrain changes in the seasonality of the Southern Ocean N cycle, the use of multispecies foraminifer-bound $\delta^{15}N$ records may prove helpful. Sediment traps from the Pacific sector and other regions suggest a consistent seasonal succession of species for the Southern Ocean region between the STF and the PF possibly driven, at least in part, by mixed-layer depth through its influence on food availability near the surface (King & Howard, 2001; King & Howard, 2003). For example, the high abundance of *G. bulloides* in springtime sinking fluxes and its close association with the chlorophyll maximum (Mortyn & Charles, 2003) suggest that this species may best record the initial drawdown of nitrate during the growing season. *N. pachyderma* and *N. incompta* have been found to dominate midsummer foraminiferal fluxes in the Pacific PFZ and SAZ, respectively (King & Howard, 2001; King & Howard, 2003), suggesting that these species may best represent midsummer conditions in the Southern Ocean. In the case of site ODP1090 in the northern SAZ, a constant $\delta^{15}N$ offset between *G. bulloides* and *O. universa* suggests that the $\delta^{15}N$ relationship between *G. bulloides* and assimilated nitrate has not changed appreciably through time (Martínez-García et al., 2014). In addition, coral-bound $\delta^{15}N$ records from across the SAZ (south of Tasmania and in the Drake Passage; Wang et al., 2017) exhibit a similar amplitude of glacial/interglacial $\delta^{15}N$ change to (and a relatively constant offset from) the foraminifer-bound $\delta^{15}N$ records at ODP1090. Deep sea corals rely on the flux of sinking PON into deep waters. There is no clear mechanism for their $\delta^{15}N$ to be biased by changes in the seasonality of the $\delta^{15}N$ of sinking PON, especially because corals appear to feed on suspended PON,

which is produced over time from sinking PON (Wang et al., 2014). The agreement between $\delta^{15}N$ proxies provides further support for scaling of seasonal signals through glacial-interglacial transitions, at least in the SAZ.

5. Conclusions

The N isotopes have been explored extensively as a tool for reconstructing the degree of nitrate consumption in the Southern Ocean, especially over glacial/interglacial cycles. The sinking flux out of the euphotic zone is an excellent target for $\delta^{15}N$ reconstruction because, regardless of upper ocean ammonium cycling, the total N sinking out of the euphotic zone is constrained by mass balance to approximate the $\delta^{15}N$ of the nitrate consumed in the euphotic zone (Altabet & François, 1994). This mass balance helped to motivate the early focus on bulk sedimentary N as a record of the $\delta^{15}N$ of sinking N in the past. Since then, however, the evidence for variable diagenetic alteration of bulk sediment $\delta^{15}N$ has driven the field to explore N protected within the mineral matrix of microfossils and fossils, including diatoms, deep sea corals, and planktic foraminifera. While the total N sinking out of the euphotic zone is constrained by mass balance to approximate the $\delta^{15}N$ of the N supply to the euphotic zone, this does not apply to any subfraction of the sinking N, including N contained within planktic fossils. For such proxies, modern ocean ground-truthing is particularly important to understand the degrees to which the proxies record nitrate consumption in the face of other N cycling processes at work in the surface ocean.

The data reported here support the utility of planktic foraminifera as recorders of nitrate consumption, but they also indicate the potential for lower-productivity periods to influence the $\delta^{15}N$ of foraminifer shells. Foraminifer $\delta^{15}N$ is more closely tied to the $\delta^{15}N$ of PON than to that of dissolved nitrate, consistent with foraminifera acquiring most (if not all) of their N from their diet. Our sampling periods included the late summer and the winter. While the degree of nitrate consumption influences the $\delta^{15}N$ of PON throughout the year (Altabet & François, 2001; Lourey et al., 2003), during the periods that we investigated, other processes are also important. In the late-summer, bulk particles and the foraminifera that feed upon them also reflect ammonium recycling, lowering their $\delta^{15}N$; in the winter, particle decomposition raises their $\delta^{15}N$. In terms of their influence on the $\delta^{15}N$ of foraminifera sinking to the seafloor each year, late-summer ammonium recycling appears to outweigh wintertime decomposition. Both signals are likely weak compared to that of the productive spring/midsummer (which dominates the present-day sinking flux) when bulk particle $\delta^{15}N$ and nitrate consumption are most tightly linked. This dominance of the nitrate consumption signal in the early summer and midsummer must be tested in future work by sampling at these times of year.

Departure from the current mode of seasonality in past climates (e.g., a more extended or intense ammonium recycling period during ice ages) would complicate the inference of nitrate consumption from downcore changes in fossil foraminifer $\delta^{15}N$. However, all PON in surface waters ultimately derives from the assimilation of nitrate, such that the productivity of the seasons with distinct N cycling probably scale with the amount of nitrate consumed. If so, there would be limited capacity for the $\delta^{15}N$ of foraminifera shells accumulated in deep sea sediments to be decoupled from the isotope dynamics of nitrate assimilation. Nevertheless, a more complete view of how the different seasons contribute to the annual, flux-weighted $\delta^{15}N$ of foraminifera is needed to better gauge the importance of the "nonnitrate" signal.

The ecological diversity among planktic foraminifer species could hold the key to disentangling changes in nitrate consumption from changes in the seasonal cycle. Since different species occupy specific (sometimes overlapping) depth, seasonal and trophic niches in their environment, there is potential for detailed reconstructions from multispecies foraminifer-bound $\delta^{15}N$ records. Tapping into this capability would require a comprehensive understanding of both the common and species-specific $\delta^{15}N$ signals recorded in foraminifer shell-bound organic matter. More field studies akin to the present one would serve this goal. Among the aspects called for in such future work is a great need to sample the Southern Ocean for foraminifera during the early-to-midsummer productive period, rather than after it, as was the case in this study.

Acknowledgments
The data presented here are available online (http://www.bco-dmo.org). This work was supported by the South African NRF (Grant 111090, S. M. S.); US NSF Grants 0922345, 1060947, and 1401489 (D. M. S.); the Max Planck Institute for Chemistry, Germany (S. M. S.); the South African National Antarctic Programme (Grant 93069, A. R.; Grants 105539 and 110735, S. E. F.); the South African NRF CSUR fund (Grant 105895, S. E. F); and the Swiss Polar Institute Antarctic Circumnavigation Expedition Grant, Project 12 (S. E. F.). We are grateful to the Department of Environmental Affairs, South Africa, for providing equipment and technical support for net tow deployments, as well as the to the Captain and crew of the R/V *S.A. Agulhas II* for safe voyages in winter 2015 and late summer 2016. We thank the members of the Sigman Lab (Princeton; particularly E. Kast and V. Luu) and Martínez-García Lab (MPIC; particularly N. Duprey and A. Foreman) for laboratory assistance and method development discussions; A. Plattner for help with creating Figure 1 in GMT; and H. Spero for insightful discussions. S. M. S. gratefully acknowledges hosting institutions, the Department of Earth and Environmental Sciences at Fresno State and the Department of Geological Sciences at the University of Alabama.

References

Altabet, M. A. (1988). Variations in nitrogen isotopic composition between sinking and suspended particles: Implications for nitrogen cycling and particle transformation in the open ocean. *Deep Sea Research Part A. Oceanographic Research Papers*, *35*, 535–554. https://doi.org/10.1016/0198-0149(88)90130-6

Altabet, M. A., Deuser, W. G., Honjo, S., & Stienen, S. (1991). Seasonal and depth-related changes in the source of sinking particles in the N. Atlantic. *Nature*, *354*, 136–139. https://doi.org/10.1038/354136a0

Altabet, M. A., & François, R. (1994). Sedimentary nitrogen isotopic ratio as a recorder for surface ocean nitrate utilization. *Global Biogeochemical Cycles*, *8*(1), 103–116. https://doi.org/10.1029/93GB03396

Altabet, M. A., & François, R. (2001). Nitrogen isotope biogeochemistry of the Antarctic Polar Frontal Zone at 170°W. *Deep-Sea Research Part II: Topical Studies in Oceanography*, *48*, 4247–4273. https://doi.org/10.1016/S0967-0645(01)00088-1

Altabet, M. A., & McCarthy, J. J. (1986). Vertical patterns in ^{15}N natural abundance in PON from the surface waters of warm-core rings. *Journal of Marine Research*, *44*, 185–201. https://doi.org/10.1357/002224086788460148

Altabet, M. A., & Small, L. F. (1990). Nitrogen isotopic ratios in fecal pellets produced by marine zooplankton. *Geochimica et Cosmochimica Acta*, *54*, 155–163. https://doi.org/10.1016/0016-7037(90)90203-W

Anderson, O. R., Spindler, M., Bé, A. W. H., & Hemleben, C. (1979). Trophic activity of planktonic foraminifera. *Journal of the Marine Biological Association of the United Kingdom*, *59*(3), 791–799. https://doi.org/10.1017/S002531540004577X

Bé, A. W. H. (1977). chapter An ecological, zoogeographic and taxonomic review of recent planktonic foraminifera. In *Oceanic micropaleontology* (Vol. 1, pp. 1–100). London: Academic Press.

Bé, A. W. H., & Hemleben, C. (1970). Calcification in a living planktonic foraminifer, Globigerinoides sacculifer (BRADY). *Neues Jahrbuch für Geologie und Paläontologie*, *134*(3), 221–234.

Bé, A. W. H., Hemleben, C., Anderson, O. R., & Spindler, M. (1979). Chamber formation in planktonic foraminifera. *Micropaleontology*, *25*((3), 294–307.

Bé, A. W. H., Hemleben, C., Anderson, O. R., Spindler, M., Hacunda, J., & Tuntivate-Choy, S. (1977). Laboratory and field observations of living planktonic foraminifera. *Micropaleontology*, *23*(2), 155–179. https://doi.org/10.2307/1485330

Belkin, I. M., & Gordon, A. L. (1996). Southern Ocean fronts from the Greenwich meridian to Tasmania. *Journal of Geophysical Research*, *101*(C2), 3675–3696. https://doi.org/10.1029/95JC02750

Bird, C., Darling, K. F., Russell, A. D., Davis, C. V., Fehrenbacher, J., Free, A., et al. (2017). Cyanobacterial endobionts within a major marine planktonic calcifier (*Globigerina bulloides*, Foraminifera) revealed by 16S rRNA metabarcoding. *Biogeosciences*, *14*, 901–920. https://doi.org/10.5194/bg-14-901-2017

Bird, C., Darling, K. F., Russell, A. D., Fehrenbacher, J. S., Davis, C. V., Free, A., & Ngwenya, B. T. (2018). 16S rRNA gene metabarcoding and TEM reveals different ecological strategies within the genus Neogloboquadrina (planktonic foraminifer). *PLoS ONE*, *13*(1), e0191653. https://doi.org/10.1371/journal.pone.0191653

Braman, R. S., & Hendrix, S. A. (1989). Nanogram nitrite and nitrate determination in environmental and biological materials by vanadium (iii) reduction with chemiluminescence detection. *Analytical Chemistry*, *61*(24), 2715–2718. https://doi.org/10.1021/ac00199a007

Buitenhuis, E. T., Moriarty, R., Vogt, M., Bednaršek, N., Doney, S. C., Leblanc, K., et al. (2013). MAREDAT: Toward a world atlas of MARine Ecosystem DATa. *Earth System Science Data*, *5*, 227–239. https://doi.org/10.5194/essd-5-227-2013

E. Campbell. Where three oceans meet: Nitrate isotope measurements from the South Atlantic along 34.5°S. Senior Thesis, 2016.

Casciotti, K. L., Sigman, D. M., Galanter Hastings, M., Böhlke, J. K., & Hilkert, A. (2002). Measurement of the oxygen isotopic composition of nitrate in seawater and freshwater using the denitrifier method. *Analytical Chemistry*, *74*, 4905–4912. https://doi.org/10.1021/ac020113w

Checkley, D. M., & Miller, C. A. (1989). Nitrogen isotope fractionation by oceanic zooplankton. *Deep Sea Research Part I: Oceanographic Research Papers*, *36*, 1449–1456. https://doi.org/10.1016/0198-0149(89)90050-2

Darling, K. F., & Wade, C. M. (2008). The genetic diversity of planktic foraminifera and the global distribution of ribosomal RNA genotypes. *Marine Micropaleontology*, *67*, 216–238. https://doi.org/10.1016/j.marmicro.2008.01.009

de Boyer Montégut, C., Madec, G., Fischer, A. S., Lazar, A., & Iudicone, D. (2004). Mixed layer depth over the global ocean: An examination of profile data and a profile-based climatology. *Journal of Geophysical Research*, *109*, C12003. https://doi.org/10.1029/2004JC002378

DiFiore, P. J., Sigman, D. M., Karsh, K. L., Trull, T. W., Dunbar, R. B., & Robinson, R. S. (2010). Poleward decrease in the isotope effect of nitrate assimilation across the Southern Ocean. *Geophysical Research Letters*, *37*, L17601. https://doi.org/10.1029/2010GL044090

DiFiore, P. J., Sigman, D. M., Trull, T. W., Lourey, M. J., Karsh, K., Cane, G., & Ho, R. (2006). Nitrogen isotope constraints on Subantarctic biogeochemistry. *Journal of Geophysical Research*, *111*, C08016. https://doi.org/10.1029/2005JC003216

Dorch, Q. (1990). The interaction between ammonium and nitrate uptake in phytoplankton. *Marine Ecology Progress Series*, *61*, 183–201. https://doi.org/10.3354/meps061183

Elskens, M., Baeyens, W., Cattaldo, T., Dehairs, F., & Griffiths, B. (2002). N uptake conditions during summer in the Subantarctic and Polar Frontal Zones of the Australian sector of the Southern Ocean. *Journal of Geophysical Research*, *107*(11), 3182. https://doi.org/10.1029/2001JC000897

Faber, W. W., Anderson, O. R., Lindsey, J. L., & Caron, D. A. (1988). Algal-foraminiferal symbiosis in the planktonic foraminifer Globigerinella aequilateralis: I. Occurrence and stability of two mutually exclusive chrysophyte endosymbionts and their ultrastructure. *Journal of Foraminiferal Research*, *18*, 334–343. https://doi.org/10.2113/gsjfr.18.4.334

Fehrenbacher, J. S., Russell, A. D., Davis, C. V., Spero, H. J., Chu, E., & Hönisch, B. (2018). Ba/Ca ratios in the non-spinose planktic foraminifer *Neogloboquadrina dutertrei*: Evidence for an organic aggregate microhabitat. *Geochimica et Cosmochimica Acta*, *236*, 361–372. https://doi.org/10.1016/j.gca.2018.03.008

François, R., Altabet, M. A., & Burckle, L. H. (1992). Glacial to interglacial changes in surface nitrate utilization in the Indian sector of the Southern Ocean as recorded by sediment $\delta^{15}N$. *Paleoceanography*, *7*(5), 589–606. https://doi.org/10.1029/92PA01573

François, R., Altabet, M. A., Yu, E. F., Sigman, D. M., Bacon, M. P., Frank, M., et al. (1997). Contribution of Southern Ocean surface-water stratification to low atmospheric CO_2 concentrations during the last glacial period. *Nature*, *389*, 929–935. https://doi.org/10.1038/40073

Fripiat, F., Martínez-García, A., Fawcett, S. E., Kemeny, P. C., Studer, A. S., Smart, S. M., et al. (2019). The isotope effect of nitrate assimilation in the Antarctic Zone: Improved estimates and paleoceanographic implications. *Geochimica et Cosmochimica Acta*, *247*, 261–279. https://doi.org/10.1016/j.gca.2018.12.003

Garcia, H. E., Locarnini, R. A., Boyer, T. P., Antonov, J. I., Baranova, O. K., Zweng, M. M., et al. (2014). Dissolved inorganic nutrients (phosphate, nitrate, silicate). In S. Levitus (Ed.), a. Mishonov technical ed.*World ocean atlas 2013*, NOAA Atlas nesdis 76 (Vol. *4*, pp. 1–25). Silver Spring, MD: National Oceanographic Data Center.

Gastrich, M. D. (1987). Ultrastructure of a new intracellular symbiotic alga found within planktonic foraminifera. *Journal of Phycology*, *23*, 623–632. https://doi.org/10.1111/j.1529-8817.1987.tb04215.x

Glibert, P. M., Biggs, D. C., & McCarthy, J. J. (1982). Utilization of ammonium and nitrate during austral summer in the Scotia Sea. *Deep Sea Research Part I: Oceanographic Research Papers*, *29*, 837–850. https://doi.org/10.1016/0198-0149(82)90049-8

Granger, J., & Sigman, D. M. (2009). Removal of nitrite with sulfamic acid for nitrate N and O isotope analysis with the denitrifier method. *Rapid Communications in Mass Spectrometry*, *23*(23), 3753–3762. https://doi.org/10.1002/rcm.4307

Gruber, N., & Sarmiento, J. L. (1997). Global patterns of marine nitrogen fixation and denitrification. *Global Biogeochemical Cycles*, *11*(2), 235–266. https://doi.org/10.1029/97GB00077

Hannides, C. C. S., Popp, B. N., Choy, C. A., & Drazen, J. C. (2013). Midwater zooplankton and suspended particle dynamics in the North Pacific subtropical gyre: A stable isotope perspective. *Limnology and Oceanography*, *58*(6), 1931–1946. https://doi.org/10.4319/lo.2013.58.6.1931

Hemleben, C., Spindler, M., & Anderson, O. R. (1989). *Modern planktonic foraminifera*. Berlin: Springer-Verlag. https://doi.org/10.1007/978-1-4612-3544-6

Hemleben, C., Spindler, M., Breitinger, I., & Deuser, W. G. (1985). Field and laboratory studies on the ontogeny and ecology of some globorotaliid species from the Sargasso Sea off Bermuda. *Journal of Foraminefera Research*, *15*(4), 254–272. https://doi.org/10.2113/gsjfr.15.4.254

Holliday, N. P., & Read, J. F. (1998). Surface oceanic fronts between Africa and Antarctica. *Deep Sea Research Part I: Oceanographic Research Papers*, *45*, 217–238. https://doi.org/10.1016/S0967-0637(97)00081-2

Honjo, S., Francois, R., Manganini, S., Dymond, J., & Collier, R. (2000). Particle fluxes to the interior of the Southern Ocean in the Western Pacific sector along 170°W. *Deep Sea Research Part II: Topical Studies in Oceanography*, *47*, 3521–3548. https://doi.org/10.1016/S0967-0645(00)00077-1

Joubert, W. R., Thomalla, S. J., Waldron, H. N., Lucas, M. I., Boye, M., Le Moigne, F. A. C., et al. (2011). Nitrogen uptake by phytoplankton in the Atlantic sector of the Southern Ocean during late austral summer. *Biogeosciences*, *8*, 2947–2959. https://doi.org/10.5194/bg-8-2947-2011

Kemeny, P. C., Kast, E. R., Hain, M. P., Fawcett, S. E., Fripiat, F., Studer, A. S., et al. (2018). A seasonal model of nitrogen isotopes in the ice age Antarctic Zone: Support for weakening of the Southern Ocean upper overturning cell. *Paleoceanography and Paleoclimatology*, *33*(12), 1453–1471. https://doi.org/10.1029/2018PA003478

Kemeny, P. C., Weigand, M. A., Zhang, R., Carter, B. R., Karsh, K. L., Fawcett, S. E., & Sigman, D. M. (2016). Enzyme-level interconversion of nitrate and nitrite in the fall mixed layer of the Antarctic Ocean. *Global Biogeochemical Cycles*, *30*, 1069–1085. https://doi.org/10.1002/2015GB005350

King, A. L., & Howard, W. R. (2003). Planktonic foraminiferal flux seasonality in Subantarctic sediment traps: A test for paleoclimate reconstructions. *Paleoceanography*, *18*(1), 1019. https://doi.org/10.1029/2002PA000839

King, K. Jr., & Hare, P. E. (1972). Amino acid composition of the test as a taxonomic character for living and fossil planktonic foraminifera. *Micropaleontology*, *18*(3), 285–293. https://doi.org/10.2307/1485009

King, A. L., & Howard, W. R. (2001). Seasonality of foraminiferal flux in sediment traps at Chatham Rise, SW Pacific: Implications for paleotemperature estimates. *Deep Sea Research Part I: Oceanographic Research Papers*, *48*, 1687–1708. https://doi.org/10.1016/S0967-0637(00)00106-0

Knapp, A. N., Sigman, D. M., & Lipschultz, F. (2005). N isotopic composition of dissolved organic nitrogen and nitrate at the Bermuda Atlantic Time-series Study site. *Global Biogeochemical Cycles*, *19*, GB1018. https://doi.org/10.1029/2004GB002320

Knox, F., & McElroy, M. B. (1984). Changes in atmospheric CO_2: Influence of the marine biota at high latitude. *Journal of Geophysical Research*, *89*, 4629–4637. https://doi.org/10.1029/JD089iD03p04629

Koike, I., Holm-Hansen, O., & Biggs, D. C. (1986). Inorganic nitrogen metabolism by Antarctic phytoplankton with special reference to ammonium cycling. *Marine Ecology Progress Series*, *30*, 105–116. https://doi.org/10.3354/meps030105

P. Kovesi. Good colour maps: How to design them. CoRR, abs/1509.03700, 2015. URL http://arxiv.org/abs/1509.03700.

Le Kieffre, C., Spero, H., Russell, A., Fehrenbacher, J., Geslin, E., & Meibom, A. (2018). Assimilation, translocation, and utilization of carbon between photosynthetic symbiotic dinoflagellates and their planktic foraminifera host. *Marine Biology*, *165*(104), 15. https://doi.org/10.1007/s00227-018-3362-7

Lehmann, M. F., Bernasconi, S. M., Barbieri, A., & McKenzie, J. A. (2002). Preservation of organic matter and alteration of its carbon and nitrogen isotope composition during simulated and in situ early sedimentary diagenesis. *Geochimica et Cosmochimica Acta*, *66*(20), 3573–3584. https://doi.org/10.1016/S0016-7037(02)00968-7

Lourey, M. J., Trull, T. W., & Sigman, D. M. (2003). Sensitivity of $\delta^{15}N$ of nitrate, surface suspended and deep sinking particulate nitrogen to seasonal nitrate depletion in the Southern Ocean. *Global Biogeochemical Cycles*, *17*(3), 1081. https://doi.org/10.1029/2002GB001973

Lutjeharms, J. R. E., & Valentine, H. R. (1984). Southern ocean thermal fronts south of Africa. *Deep Sea Research Part A. Oceanographic Research Papers*, *31*, 1461–1475. https://doi.org/10.1016/0198-0149(84)90082-7

Martin, J. H. (1990). Glacial-interglacial CO_2 change: The iron hypothesis. *Paleoceanography*, *5*(1), 1–13. https://doi.org/10.1029/PA005i001p00001

Martínez-García, A., Sigman, D. M., Ren, H., Anderson, R. F., Straub, M., Hodell, D. A., et al. (2014). Iron fertilization of the Subantarctic ocean during the last ice age. *Science*, *343*(6177), 1347–1350. https://doi.org/10.1126/science.1246848

Martiny, A. C., Vrugt, J. A., & Lomas, M. W. (2014). Concentrations and ratios of particulate organic carbon, nitrogen, and phosphorus in the global ocean. *Scientific Data*, *1*, 140048. https://doi.org/10.1038/sdata.2014.48

McCartney, M. S. (1977). chapter Subantarctic Mode Water. In *A voyage of discovery: George Deacon 70th anniversary volume* (pp. 103–119. Supplement to Deep-Sea Research). Oxford: Pergamon Press.

McNeil, B. I., Matear, R. J., & Tilbrook, B. (2001). Does carbon 13 track anthropogenic CO_2 in the Southern Ocean? *Global Biogeochemical Cycles*, *15*, 597–613. https://doi.org/10.1029/2000GB001352

Meilland, J., Siccha, M., Weinkauf, M. F. G., Jonkers, L., Morard, R., Baranowski, U., et al. (2019). Highly replicated sampling reveals no diurnal vertical migration but stable species-specific vertical habitats in planktonic foraminifera. *Journal of Plankton Research*, *41*(2), 127–141. https://doi.org/10.1093/plankt/fbz002

Minagawa, M., & Wada, E. (1984). Stepwise enrichment of 15 N along food chains: Further evidence and the relation between d15N and animal age. *Geochimica et Cosmochimica Acta*, *48*, 1135–1140. https://doi.org/10.1016/0016-7037(84)90204-7

Möbius, J. (2013). Isotope fractionation during nitrogen remineralization (ammonification): Implications for nitrogen isotope biogeochemistry. *Geochimica et Cosmochimica Acta*, *105*, 422–432. https://doi.org/10.1016/j.gca.2012.11.048

Mortyn, P. G., & Charles, C. D. (2003). Planktonic foraminiferal depth habitat and $\delta^{18}O$ calibrations: Plankton tow results from the Atlantic sector of the Southern Ocean. *Paleoceanography*, *18*(2), 1037. https://doi.org/10.1029/2001PA000637

Nakagawa, S., & Schielzeth, H. (2013). A general and simple method for obtaining R2 from generalized linear mixed-effects models. *Methods in Ecology and Evolution*, *4*(2), 133–142. https://doi.org/10.1111/j.2041-210x.2012.00261.x

Nodder, S. D., & Northcote, L. C. (2001). Episodic particulate fluxes at southern temperate midlatitudes (42–45°S) in the Subtropical Front region, east of New Zealand. *Deep Sea Research Part I: Oceanographic Research Papers*, *48*(3), 833–864. https://doi.org/10.1016/S0967-0637(00)00062-5

Nowlin, W. D., & Klinck, J. M. (1986). The physics of the Antarctic Circumpolar Current. *Reviews of Geophysics*, *24*(3), 469–491. https://doi.org/10.1029/RG024i003p00469

Nydahl, F. (1978). On the peroxodisulphate oxidation of total nitrogen in waters to nitrate. *Water Research*, *12*, 1123–1130. https://doi.org/10.1016/0043-1354(78)90060-X

Pennock, J. R., Velinsky, D. J., Ludlam, J. M., Sharp, J. H., & Fogel, M. L. (1996). Isotope fractionation of ammonium and nitrate during their uptake by Skeletonema Costatum: Implications for the $\delta^{15}N$ dynamics under bloom conditions. *Limnology and Oceanography*, *41*(3), 451–459. https://doi.org/10.4319/lo.1996.41.3.0451

Philibert, R., Clark, D. R., & Waldron, H. N. (2015). A geographical and seasonal comparison of nitrogen uptake by phytoplankton in the Southern Ocean. *Ocean Science*, *11*, 251–267. https://doi.org/10.5194/os-11-251-2015

Pinheiro, J., & Bates, D. (2000). *Mixed-Effects Models in S and S-PLUS*. New York, NY: Springer-Verlag.

Qi, H., Coplen, T. B., Geilmann, H., Brand, W. A., & Böhlke, J. K. (2003). Two new organic reference materials for $\delta^{13}C$ and $\delta^{15}N$ measurements and a new value for the $\delta^{13}C$ of NBS 22 oil. *Rapid Communications in Mass Spectrometry*, *17*(22), 2483–2487. https://doi.org/10.1002/rcm.1219

Rafter, P. A., DiFiore, P. J., & Sigman, D. M. (2013). Coupled nitrate nitrogen and oxygen isotopes and organic matter remineralization in the Southern and Pacific Oceans. *Journal of Geophysical Research: Oceans*, *118*, 4781–4794. https://doi.org/10.1002/jgrc.20316

Rafter, P. A., Sigman, D. M., Charles, C. D., Kaiser, J., & Haug, G. H. (2012). Subsurface tropical Pacific nitrogen isotopic composition of nitrate: Biogeochemical signals and their transport. *Global Biogeochemical Cycles*, *26*, GB1003. https://doi.org/10.1029/2010GB003979

Ren, H., Sigman, D. M., Meckler, A. N., Plessen, B., Robinson, R. S., Rosenthal, Y., & Haug, G. H. (2009). Foraminiferal isotope evidence of reduced nitrogen fixation in the ice age Atlantic Ocean. *Science*, *323*(5911), 244–248. https://doi.org/10.1126/science.1165787

Ren, H., Sigman, D. M., Thunell, R. C., & Prokopenko, M. G. (2012). Nitrogen isotopic composition of planktonic foraminifera from the modern ocean and recent sediments. *Limnology and Oceanography*, *57*(4), 1011–1024. https://doi.org/10.4319/lo.2012.57.4.1011

Robinson, R. S., Brunelle, B. G., & Sigman, D. M. (2004). Revisiting nutrient utilization in the glacial Antarctic: Evidence from a new diatom-bound N isotope method. *Paleoceanography*, *19*, PA3001. https://doi.org/10.1029/2003PA000996

Robinson, R. S., Kienast, M., Albuquerque, A. L., Altabet, M., Contreras, S., Holz, R. D. P., et al. (2012). A review of nitrogen isotopic alteration in marine sediments. *Paleoceanography*, *27*, PA4203. https://doi.org/10.1029/2012PA002321

Saino, T., & Hattori, A. (1980). ^{15}N natural abundance in oceanic suspended particulate matter. *Nature*, *283*, 752–754. https://doi.org/10.1038/283752a0

Sambrotto, R. N., & Mace, B. J. (2000). Coupling of biological and physical regimes across the Antarctic Polar Front as reflected by nitrogen production and recycling. *Deep Sea Research Part II: Topical Studies in Oceanography*, *47*(15-16), 3339–3367. https://doi.org/10.1016/S0967-0645(00)00071-0

C. Sandrock and S. Afshari. Plot ternary diagrams in MATLAB. 2016. https://doi.org/10.5281/zenodo.166760. [Data set].

Sarmiento, J. L., & Toggweiler, J. R. (1984). A new model for the role of the oceans in determining atmospheric pCO_2. *Nature*, *308*, 621–624. https://doi.org/10.1038/308621a0

Schiebel, R. (2002). Planktic foraminiferal sedimentation and the marine calcite budget. *Global Biogeochemical Cycles*, *16*(4), 1065. https://doi.org/10.1029/2001GB001459

Schiebel, R., & Hemleben, C. (2017). *Planktic Foraminifers in the Modern Ocean*. Berlin Heidelberg: Springer-Verlag. https://doi.org/10.1007/978-3-662-50297-6

Schiebel, R., Smart, S. M., Jentzen, A., Jonkers, L., Morard, R., Meilland, J., et al. (2018). Advances in planktonic foraminifer research: New perspectives for paleoceanography. *Revue de Micropaleontologie*, *61*(3-4), 113–138. https://doi.org/10.1016/j.revmic.2018.10.001

Schiebel, R., Waniek, J., Zeltner, A., & Alves, M. (2002). Impact of the Azores Front on the distribution of planktic foraminifers, shelled gastropods, and coccolithophorids. *Deep Sea Research Part II: Topical Studies in Oceanography*, *49*, 4035–4050. https://doi.org/10.1016/S0967-0645(02)00141-8

Sicchа, M., Schiebel, R., Schmidt, S., & Howa, H. (2012). Short-term and small-scale variability in planktic foraminifera test flux in the Bay of Biscay. *Deep Sea Research Part I: Oceanographic Research Papers*, *64*, 146–156. https://doi.org/10.1016/j.dsr.2012.02.004

Siegenthaler, U., & Wenk, T. (1984). Rapid atmospheric CO_2 variations and ocean circulation. *Nature*, *308*, 624–626. https://doi.org/10.1038/308624a0

Sigman, D. M., Altabet, M. A., François, R., McCorkle, D. C., & Gaillard, J. F. (1999). The isotopic composition of diatom-bound nitrogen in Southern Ocean sediments. *Paleoceanography*, *14*(2), 118–134. https://doi.org/10.1029/1998PA900018

Sigman, D. M., Altabet, M. A., McCorkle, D. C., François, R., & Fischer, G. (1999). The $\delta^{15}N$ of nitrate in the Southern Ocean: Consumption of nitrate in surface waters. *Global Biogeochemical Cycles*, *13*(4), 1149–1166. https://doi.org/10.1029/1999GB900038

Sigman, D. M., Altabet, M. A., McCorkle, D. C., François, R., & Fischer, G. (2000). The $\delta^{15}N$ of nitrate in the Southern Ocean: Nitrogen cycling and circulation in the ocean interior. *Journal of Geophysical Research*, *105*(C8), 19,599–19,614. https://doi.org/10.1029/2000JC000265

Sigman, D. M., Casciotti, K. L., Andreani, M., Barford, C., Galanter, M., & Böhlke, J. K. (2001). A bacterial method for the nitrogen isotopic analysis of nitrate in seawater and freshwater. *Analytical Chemistry*, *73*(17), 4145–4153. https://doi.org/10.1021/ac010088e

K.Y. Sinyanya, R.G. Parrott, R.F. Flynn, D.R. Walker, Y. Ryu, D.M. Sigman, and S.E. Fawcett. The Agulhas Current enhances the productivity of the subtropical Indian Ocean: Evidence from coupled flow cytometry-high sensitivity nitrogen isotope analysis. Ocean Sciences Meeting, February 2020. American Geophysical Union.

Smart, S. M. (2014). *Wintertime nitrate isotope dynamics in the Atlantic sector of the Southern Ocean. Master's thesis*. South Africa: University of Cape Town.

Smart, S. M., Fawcett, S. E., Thomalla, S. J., Weigand, M. A., Reason, C. J. C., & Sigman, D. M. (2015). Isotopic evidence for nitrification in the Antarctic winter mixed layer. *Global Biogeochemical Cycles*, *29*, 427–445. https://doi.org/10.1002/2014GB005013

Smart, S. M., Ren, H., Fawcett, S. E., Schiebel, R., Conte, M., Rafter, P. A., et al. (2018). Ground-truthing the planktic foraminifer-bound nitrogen isotope paleo-proxy in the Sargasso Sea. *Geochimica et Cosmochimica Acta*, *235*, 463–482. https://doi.org/10.1016/j.gca.2018.05.023

Speer, K., Rintoul, S. R., & Sloyan, B. (2000). The diabatic Deacon cell. *Journal of Physical Oceanography*, *30*, 3212–3222. https://doi.org/10.1175/1520-0485(2000)030<3212:TDDC>2.0.CO;2

Spero, H. (1987). Symbiosis in the planktonic foraminifer, *Orbulina universa*, and the isolation of its symbiotic dinoflagellate, *Gymnodinium béii* sp. NOV.1. *Journal of Phycology*, *23*, 307–317. https://doi.org/10.1111/j.1529-8817.1987.tb04139.x

Spero, H. J. (1988). Ultrastructural examination of chamber morphogenesis and biomineralization in the planktonic foraminifer *Orbulina universa*. *Marine Biology*, *99*(1), 9–20. https://doi.org/10.1007/BF00644972

Spero, H. J., & Angel, D. L. (1991). Planktonic sarcodines: Microhabitat for oceanic dinoflagellates. *Journal of Phycology*, *27*, 187–195. https://doi.org/10.1111/j.0022-3646.1991.00187.x

Spindler, M., Hemleben, C., Salomons, J., & Smit, L. (1984). Feeding behavior of some planktonic foraminifers in laboratory cultures. *Journal of Foraminiferal Research*, *14*(4), 237–249. https://doi.org/10.2113/gsjfr.14.4.237

Stoecker, D. K., Hansen, P. J., Caron, D. A., & Mitra, A. (2017). Mixotrophy in the marine plankton. *Annual Review of Marine Science*, *9*, 311–335. https://doi.org/10.1146/annurev-marine-010816-060617

Stoecker, D. K., Johnson, M. D., de Vargas, C., & Not, F. (2009). Acquired phototrophy in aquatic protists. *Aquatic Microbial Ecology*, *57*(3), 279–310. https://doi.org/10.3354/ame01340

Studer, A. S., Sigman, D. M., Martínez-García, A., Benz, V., Winckler, G., Kuhn, G., et al. (2015. ISSN 1944-9186). Antarctic zone nutrient conditions during the last two glacial cycles. *Paleoceanography*, *30*, 845–862. https://doi.org/10.1002/2014PA002745

Studer, A. S., Sigman, D. M., Martínez-García, A., Thöle, L. M., Michel, E., Jaccard, S. L., et al. (2018). Increased nutrient supply to the Southern Ocean during the Holocene and its implications for the pre-industrial atmospheric CO_2 rise. *Nature Geoscience*, *11*(10), 756–760. https://doi.org/10.1038/s41561-018-0191-8

Takagi, H., Kimoto, K., Fujiki, T., Saito, H., Schmidt, C., Kucera, M., & Moriya, K. (2019). Characterizing photosymbiosis in modern planktonic foraminifera. *Biogeosciences*, *16*(17), 3377–3396. https://doi.org/10.5194/bg-2019-145

Thomalla, S. J., Waldron, H. N., Lucas, M. I., Read, J. F., Ansorge, I. J., & Pakhomov, E. (2011). Phytoplankton distribution and nitrogen dynamics in the southwest Indian subtropical gyre and Southern Ocean waters. *Ocean Science*, *7*, 113–127. https://doi.org/10.5194/os-7-113-2011

Thunell, R. C., Sigman, D. M., Muller-Karger, F., Astor, Y., & Varela, R. (2004). Nitrogen isotope dynamics of the Cariaco Basin, Venezuela. *Global Biogeochemical Cycles*, *18*, GB3001. https://doi.org/10.1029/2003GB002185

Toole, J. M. (1981). Sea ice, winter convection, and the temperature minimum layer in the Southern Ocean. *Journal of Geophysical Research*, *86*(C9), 8037–8047. https://doi.org/10.1029/JC086iC09p08037

Trull, T., Bray, S., Manganini, S., Honjo, S., & François, R. (2001). Moored sediment trap measurements of carbon export in the Sub-Antarctic and Polar Frontal zones of the Southern Ocean, south of Australia. *Journal of Geophysical Research*, *106*(C12), 31,489–31,509. https://doi.org/10.1029/2000JC000308

Trull, T. W., Davies, D., & Casciotti, K. (2008). Insights into nutrient assimilation and export in naturally iron-fertilized waters of the Southern Ocean from nitrogen, carbon and oxygen isotopes. *Deep Sea Research Part II: Topical Studies in Oceanography*, *55*, 820–840. https://doi.org/10.1016/j.dsr2.2007.12.035

Uhle, M. E., Macko, S. A., Spero, H. J., Engel, M. H., & Lea, D. W. (1997). Sources of carbon and nitrogen in modern planktonic foraminifera: The role of algal symbionts as determined by bulk and compound specific stable isotopic analyses. *Organic Geochemistry*, *27*(3/4), 103–113. https://doi.org/10.1016/0198-0149(89)90050-2

Uhle, M. E., Macko, S. A., Spero, H. J., Lea, D. W., Ruddiman, W. F., & Engel, M. H. (1999). The fate of nitrogen in the *Orbulina universa* foraminifera–symbiont system determined by nitrogen isotope analyses of shell-bound organic matter. *Limnology and Oceanography*, *44*(8), 1968–1977. https://doi.org/10.4319/lo.1999.44.8.1968

Wada, E., & Hattori, A. (1978). Nitrogen isotope effects in the assimilation of inorganic nitrogenous compounds by marine diatoms. *Geomicrobiology Journal*, *1*(1), 85–101. https://doi.org/10.1080/01490457809377725

Wang, X. T., Prokopenko, M. G., Sigman, D. M., Adkins, J. F., Robinson, L. F., Ren, H., et al. (2014). Isotopic composition of carbonate-bound organic nitrogen in deep-sea scleractinian corals: A new window into past biogeochemical change. *Earth and Planetary Science Letters*, *400*, 243–250. https://doi.org/10.1016/j.epsl.2014.05.048

Wang, X. T., Sigman, D. M., Prokopenko, M. G., Adkins, J. F., Robinson, L. F., Hines, S. K., et al. (2017). Deep-sea coral evidence for lower Southern Ocean surface nitrate concentrations during the last ice age. *Proceedings of the National Academy of Sciences*, *114*(13), 3352–3357. https://doi.org/10.1073/pnas.1615718114

Waser, N. A. D., Harrison, P. J., Nielsen, B., Calvert, S. E., & Turpin, D. H. (1998). Nitrogen isotope fractionation during the uptake and assimilation of nitrate, nitrite, ammonium, and urea by a marine diatom. *Limnology and Oceanography*, *43*(2), 215–224. https://doi.org/10.4319/lo.1998.43.2.0215

Weigand, M. A., Foriel, J., Barnett, B., Oleynik, S., & Sigman, D. M. (2016). Updates to instrumentation and protocols for isotopic analysis of nitrate by the denitrifier method. *Rapid Communications in Mass Spectrometry*, *30*(12), 1365–1383. https://doi.org/10.1002/rcm.7570

Wessel, P., Smith, W. H. F., Scharroo, R., Luis, J., & Wobbe, F. (2013. ISSN 2324-9250). Generic mapping tools: Improved version released. *Eos, Transactions American Geophysical Union*, *94*(45), 409–410. https://doi.org/10.1002/2013EO450001

Weyl, P. K. (1978). Micropaleontology and ocean surface climate. *Science*, *202*(4367), 475–481. https://doi.org/10.1126/science.202.4367.475

Wu, J., Calvert, S. E., & Wong, C. S. (1997). Nitrogen isotope variations in the subarctic northeast Pacific: relationships to nitrate utilization and trophic structure. *Deep Sea Research Part I: Oceanographic Research Papers*, *44*(2), 287–314. https://doi.org/10.1016/S0967-0637(96)00099-4